A Spatiotemporal Notch Interaction Map from Membrane to Nucleus

Alexandre P. Martin[1], Gary A. Bradshaw[2], Robyn J. Eisert[1], Emily D. Egan[1], Lena Tveriakhina[1], Julia M. Rogers[1], Andrew N. Dates[1], Gustavo Scanavachi[3,4], Jon C. Aster[5], Tom Kirchhausen[3,4], Marian Kalocsay[6*], Stephen C. Blacklow[1,7,8*]

[1]Department of Biological Chemistry and Molecular Pharmacology, Blavatnik Institute, Harvard Medical School, Boston, MA 02115, USA.
[2]Department of Systems Biology, Laboratory of Systems Pharmacology, Harvard Medical School, Boston, MA 02115, USA.
[3]Department of Cell Biology, Harvard Medical School, Boston, MA 02115, USA.
[4]Program in Cellular and Molecular Medicine, Boston Children's Hospital, Boston, MA 02115, USA; Department of Pediatrics, Harvard Medical School, Boston, MA 02115, USA.
[5]Department of Pathology, Brigham and Women's Hospital, Boston, MA 02115, USA.
[6]Department of Experimental Radiation Oncology, University of Texas MD Anderson Cancer Center, Houston, TX 77030, USA.
[7]Department of Cancer Biology, Dana Farber Cancer Institute, Boston, MA 02215, USA.
[8]Lead contact

*Correspondence: mkalocsay@mdanderson.org (M.K.), stephen_blacklow@hms.harvard.edu (S.C.B.)

ABSTRACT

Notch signaling relies on ligand-induced proteolysis to liberate a nuclear effector that drives cell fate decisions. The location and timing of individual steps required for proteolysis and movement of Notch from membrane to nucleus, however, remain unclear. Here, we use proximity labeling with quantitative multiplexed mass spectrometry to monitor the microenvironment of endogenous Notch2 after ligand stimulation in the presence of a gamma secretase inhibitor and then as a function of time after inhibitor removal. Our studies show that gamma secretase cleavage of Notch2 occurs in an intracellular compartment and that formation of nuclear complexes and recruitment of chromatin-modifying enzymes occurs within 45 minutes of inhibitor washout. This work provides a spatiotemporal map of unprecedented detail tracking the itinerary of Notch from membrane to nucleus after activation and identifies molecular events in signal transmission that are potential targets for modulating Notch signaling activity.

INTRODUCTION

Notch signaling is an essential and conserved mechanism of cell-cell communication that controls normal development and maintains adult tissue homeostasis in a wide range of tissues and organ systems (Hori et al., 2013; Siebel & Lendahl, 2017). Mutations in Notch signaling components result in several human developmental disorders such as Alagille syndrome, caused by loss of function mutations of either *NOTCH2* or *JAGGED1* (Kamath et al., 2012; Li et al., 1997), spondylocostal dysostosis (Turnpenny et al., 2003), and Hajdu-Cheney disease (Simpson et al., 2011). In addition, Notch mutations and/or deregulated Notch signaling are frequently found in cancer (Aster et al., 2016). Activating mutations of *NOTCH1* occur in more than 50% of T cell acute lymphoblastic leukemias (T-ALL), and similar activating mutations have been found in triple-negative breast cancer, adenoid cystic carcinoma, and tumors derived from pericytes or smooth muscle (Aster et al., 2016). On the other hand, Notch acts as a tumor suppressor in cutaneous squamous cell carcinomas (N. J. Wang et al., 2011), highlighting the complexities in targeting Notch for cancer therapy.

Notch proteins (Notch1-4 in mammals) are transmembrane receptors that transmit signals in response to canonical Delta-like or Jagged ligands (Jagged1, Jagged2, DLL1, DLL4) present on a signal-sending cell. Ligand binding initiates signal transduction by triggering a series of proteolytic cleavages of Notch in the receiver cell. The first ligand-induced cleavage is catalyzed by ADAM10 at a site called S2, external to the plasma membrane. S2-cleaved Notch molecules are then cleaved by gamma secretase at site S3, resulting in the release of the Notch intracellular domain (NICD). NICD subsequently translocates into the nucleus and forms a Notch transcription complex with the DNA-binding protein RBPJ and a MAML coactivator to induce the transcription of Notch target genes (see (Henrique & Schweisguth, 2019) and (Sprinzak & Blacklow, 2021) for recent reviews).

While these fundamental steps required for Notch signaling have been defined, it is less certain where gamma secretase cleavage takes place in the cell, whether NICD moves from membrane to nucleus by active or passive transport, and how long it takes NICD to migrate from membrane to nucleus after gamma secretase cleavage. Real-time luciferase complementation assays using ectopic expression of Notch1 and RBPJ fusion proteins have shown that immobilized ligand stimulation results in nuclear complementation between 30 – 60 min after removal of a

gamma secretase inhibitor (Ilagan et al., 2011), but analogous experiments have not been carried out at endogenous protein abundance. Previous reports have also reached different conclusions, for example, about whether gamma secretase cleavage occurs at the plasma membrane (Chyung et al., 2005; Hansson et al., 2005) or in an intracellular compartment (Chapman et al., 2016; Gupta-Rossi et al., 2004; Kobia et al., 2014).

To address these questions, we mapped the microenvironment of NICD and characterized its interactions with effectors within a native cellular environment at endogenous expression levels after ligand stimulation in the presence of a gamma secretase inhibitor (GSI) and then as a function of time after inhibitor removal. We used CRISPR/Cas9 genome editing in SVG-A cells to fuse the Notch2 receptor to the engineered ascorbate peroxidase APEX2, which rapidly produces short-lived biotin-tyramide radicals that label proteins within a small radius (~ 20 nm) and that can be rapidly quenched (Hung et al., 2016; Lam et al., 2015; Rhee et al., 2013). We performed proximity labeling of the Notch2 microenvironment after ligand stimulation in the presence of a GSI and at different timepoints after inhibitor washout to identify changes in protein enrichment as a function of time by quantitative multiplexed proteomics. The dynamics of labeling enrichment of distinct plasma membrane, cytosolic, and nuclear proteins define the microenvironment of Notch2-APEX2 during its passage from the plasma membrane to the nucleus. Our studies show that gamma secretase cleavage of Notch2 to produce NICD2 occurs in an intracellular compartment, that passage of NICD2 through the cytoplasm is associated with transient enrichment of membrane cortical and cytoskeletal proteins, and that formation of nuclear complexes and recruitment of chromatin-modifying enzymes occurs within 45 minutes of inhibitor washout. This work provides a spatiotemporal map of unprecedented detail tracking the itinerary of Notch from membrane to nucleus after metalloprotease cleavage and uncovers events in signal transmission that are potential targets for modulating Notch activity.

RESULTS

System validation and genome engineering for Notch2 proximity labeling in SVG-A cells

To track the movement of Notch as a function of time in response to signal induction, we labeled proteins in the Notch microenvironment using a Notch2-APEX2 ascorbate peroxidase fusion protein (Martin et al., 2019; May et al., 2021; Paek et al., 2017). We investigated the

response associated with the Notch2/Jagged1 (Jag1) receptor-ligand pair because this pairing transmits signals that are required for normal development (Siebel & Lendahl, 2017), as highlighted by Alagille syndrome, a multiorgan disorder caused by loss-of-function mutations in either *NOTCH2* or *JAGGED1* (Kamath et al., 2012; Li et al., 1997). To achieve the precise synchronization necessary for time-resolved proximity labeling, we used immobilized Jag1 as an activating ligand in concert with potent, specific gamma secretase inhibitors, the effects of which can be rapidly reversed by simple washout (Bailis et al., 2014). We selected SVG-A human fetal astrocytes as our receptor-expressing cells ("Notch" or "receiver" cells) because they express abundant Notch2 endogenously and express low amounts of the other Notch receptors. We confirmed that Notch2 is responsible for the Notch transcriptional response in these cells by knocking out Notch2 using CRISPR/Cas9 genome editing (Ran et al., 2013): the absence of Notch2 effectively abolishes Notch reporter gene activity in a signaling assay using immobilized Jag1 as ligand (Figure S1A-B), confirming both that these cells are responsive to Jag1 and that the reporter signal in these cells is a consequence of Notch2 activation.

To ensure that our studies were performed at natural receptor abundance, we used CRISPR/Cas9 to add an APEX2-HA coding sequence to the 3' end of *NOTCH2*, creating a fusion gene at the endogenous locus encoding Notch2 fused to APEX2-HA at its C-terminus (Figure S1). The cassette for homologous recombination also contained a T2A sequence followed by a sequence encoding the mNEONGreen fluorescent protein, allowing us to isolate single cells positive for the desired genomic insertion by FACS. We confirmed that the Notch2-APEX2-HA fusion protein matures similarly to wild-type Notch2 in parental cells (Figure S1D), retains signaling activity in response to immobilized Jag1 comparable to wild-type Notch2 in a reporter gene assay, and is silenced similarly to wild-type Notch2 by inhibitors of ADAM10 and gamma secretase cleavage (Figure S1E). Western blot analysis also confirmed that biotinylation of proteins across a wide range of molecular weights was only observed in cells carrying the APEX2 fusion protein (Figure S1F).

Time-resolved Notch2 proximity labeling with the APEX2 fusion protein

We cultured Notch2-APEX2-HA knock-in cells on plates containing immobilized Jag1 (Delaney et al., 2005; Gordon et al., 2015; Varnum-Finney et al., 2003) overnight in the presence of the gamma secretase inhibitor Compound E (GSI) and analyzed protein biotinylation as a

function of time after GSI washout by mass spectrometry (Figure 1A-B). A condition without ligand served as a reference to determine how the Notch2 microenvironment is affected by ligand-induced metalloprotease cleavage in the presence of GSI (Figure 1B). We confirmed that GSI washout resulted in accumulation of S3-processed NICD2 molecules over a two-hour time course (Figure S2A), performed proximity labeling using biotin phenol and hydrogen peroxide at various time points up to 2 h, and by Western blot observed specific labeling of cohorts of biotin-labeled proteins that changed with time (Figure S2B).

Mass spectrometry (MS) analysis of biotinylated proteins labeled by Notch2-APEX2 (Figure S3A) determined the temporal profiles of labeling for 980 proteins, which displayed different dynamic labeling patterns after Notch activation. The high correlation between replicates (Figure S3B) and the clustering of replicates in principal component analysis (Figure S3C) attests to the reproducibility of our experimental system. When referenced to the t=0 timepoint, the transcriptional coactivator MAML1, an essential component of the Notch transcriptional complex (Petcherski & Kimble, 2000; Wu et al., 2000), was not significantly enriched at early timepoints after GSI washout (<30 min) but became the most significantly enriched protein two hours after GSI washout. This observation confirmed nuclear translocation of NICD2 after GSI removal and highlighted the dynamic nature of the NICD2 microenvironment as a function of time. We also note that our MS workflow did not identify all known Notch associated proteins in this study, as MS proteomics often does not capture all protein analytes present. For example, RBPJ, the transcription factor bound by NICD in the transcriptional activation complex, was not detected, even though RBPJ was indeed biotinylated as early as 30 min after GSI washout with a peak of relative abundance at 2 h after washout, as judged by Western blot (Figure S3D).

Hierarchical clustering of the relative abundance of each labeled protein as a function of time led to the identification of several distinct patterns of enrichment based on Ward's hierarchical clustering method (Figure 1C). Prominent among these enrichment patterns are seven discrete classes of proteins, including those with maximum labeling: i) in the absence of ligand, ii) with ligand in the presence of GSI, iii) early (2-5 min) in the washout time course (Figure 1D), or iv) 2 h after washout (Figure 1E). There are also proteins that are not labeled in the absence of ligand and show a sustained labeling pattern in the presence of ligand throughout the time course (Figure 1F), as well as a cluster of proteins that show enrichment both in the presence of GSI and at late

time points after washout. Full quantification data for proteins identified in this dataset are found in Table S1.

Notch2 is internalized after S2 but before S3 cleavage

Not surprisingly, the first cluster, which exhibits maximum labeling enrichment in the absence of immobilized ligand (*i*.e. when Notch is unstimulated; Figure 1C), is characterized by proteins that reside at the plasma membrane (Figure 2A-B), where Notch encounters its transmembrane ligands present on neighboring cells. This group of proteins includes EGFR (Epidermal growth factor receptor), ERBB2 (Receptor tyrosine-protein kinase erbB-2), ERBIN (Erbin), GPRC5A (Retinoic acid-induced protein 3), DBN1 (Drebrin), and surface-associated proteins such as the catenins CTNNB1 and CTNND1.

In the presence of GSI, ligand binding induces metalloprotease cleavage, but gamma secretase catalyzed cleavage at S3 is blocked, preventing liberation of NICD2 from the membrane. Remarkably, when GSI is present, plasma-membrane associated proteins, which are enriched in the first cluster when ligand is not present, become depleted when compared to unstimulated cells (Figure 2C). Instead, proteins that exhibit maximal enrichment in their proximity to Notch2 after ligand exposure in the presence of GSI are predominantly associated with vesicular or endosomal compartments and the endocytic machinery (Figure 2C-E). Core components participating in clathrin-mediated endocytosis including clathrin, AP-2, dynamin, and EPS15 are enriched (Figures 1F and 2D) as is the transferrin receptor, which enters cells through CME, and other proteins implicated in vesicular trafficking such as EHD1, SEC22B, and SNX3 (Figure 2C-E). In addition, there is a substantial enrichment of vesicle-associated TMED (transmembrane emp24 domain) proteins upon ligand stimulation (Figure 2C-D), specifically TMEM165, TMEM43. VAPA, and VAPB, two vesicle-associated proteins (Aber et al., 2019; Seaman, 2012), also show maximum enrichment in the presence of GSI (Figure 2D). Another group of proteins showed labeling enrichment in the presence of GSI that persisted after washout (Figure 2D). This group includes proteins related to endocytosis and vesicular trafficking, as well as the amyloid-beta precursor protein (APP; Figure 2D), a well-known substrate of the gamma secretase complex (Chow et al., 2010). Finally, proteins related to endocytosis and components of the clathrin-mediated endocytic machinery (Figure 2D) exhibited a significant increase in abundance upon ligand stimulation, with variable enrichment after GSI washout (Figures 1F and 2D).

The comparison between the no ligand and GSI conditions suggests that Notch2 undergoes internalization after ligand-induced ADAM10 cleavage has occurred at site S2. To evaluate this possibility using a complementary approach, we monitored the subcellular localization of Notch2 by immunofluorescence after washout of GI254023X (GI25X), a potent ADAM10 inhibitor (Ludwig et al., 2005), in the absence or presence of the dynamin inhibitor hydroxy-dynasore, which blocks endocytosis (Kirchhausen et al., 2008; Macia et al., 2006; Mccluskey et al., 2013). Cells were incubated overnight on immobilized Jagged1 in the presence of GI25X, and the inhibitor was then removed to allow S2 cleavage of ligand-bound Notch2 in the absence or presence of hydroxy-dynasore. As anticipated, washout of GI25X in the absence of the dynamin inhibitor resulted in nuclear accumulation of NICD2 by 2 h after washout (Figure 3A-C), indicating that S2 cleavage, S3 cleavage, and nuclear translocation had occurred. However, washout of GI25X in the presence of hydroxy-dynasore significantly impaired the nuclear accumulation of NICD2 (Figure 3A-C). In addition, the inhibition of endosomal acidification by bafilomycin-A1 (BafA1), a specific vacuolar H^+-ATPase inhibitor (Vaccari et al., 2010; Xu et al., 2003; Yoshimori et al., 1991), or by chloroquine (Mauthe et al., 2018), also impaired Notch2 nuclear accumulation after GI25X washout (Figure 3A-C), further suggesting that S3 cleavage required access to an acidified intracellular compartment. Importantly, none of these inhibitors significantly modified the subcellular localization of unstimulated Notch2 (Figure S4A), consistent with the conclusion that they act after ligand-induced S2 cleavage of Notch2.

The generation of the S3-cleaved form of Notch2 (NICD2) after GI25X washout was also evaluated by Western blotting, using an antibody that specifically recognizes the N-terminal epitope of NICD2 (Shanmugam et al., 2021). As expected, washout of GI25X resulted in an increase in NICD2 abundance that was greatly impaired by inhibition of endocytosis or vesicular acidification (Figure 3D-E). Finally, the effect of inhibiting endocytosis or vesicular acidification on Notch transcriptional activity was investigated using a well-characterized luciferase reporter assay (Aster et al., 2000; Rogers et al., 2020; Wu et al., 2000). Washout of GI25X induced a Notch-dependent transcriptional response that was substantially reduced by the presence of hydroxy-dynasore, BafA1, or chloroquine (Figure 3F). In contrast, however, when the same approach was used to wash out GSI, NICD2 accumulated in the nucleus after 2 h, whether or not an endocytosis or acidification inhibitor was present (Figures 3G-H and S4B), placing the step requiring endocytosis between S2 and S3 cleavage. Importantly, this sensitivity extends to other members

of the Notch receptor family, as NICD1 generation was also reduced in SVG-A cells upon the inhibition of endocytosis or vesicular acidification after GI25X washout (Figure S5A). Moreover, this sensitivity is cell line independent, as inhibitors of endocytosis or vesicular acidification reduced the generation of both NICD1 and NICD2 in 293T cells (Figure S5B), U2OS cells (Figure S5C), HeLa cells (Figure S5D), and U251 cells (Figure S5E). These results argue that bound ligand induces metalloprotease cleavage at S2 at the cell surface, and that the S2-cleaved form of Notch2 is then internalized to an intracellular compartment where it is cleaved by gamma secretase, thereby allowing NICD2 to access the nucleus.

Passage of NICD2 from membrane to nucleus

In our dataset we identified a class of proteins whose relative abundance increases shortly after GSI washout (2 - 5 minutes) (Figure 1C-D). Among the proteins in this cluster, we detected the ERM proteins ezrin (EZR), radixin (RDX), and moesin (MSN), which play a role in linking membranes to the actin cytoskeleton (Fehon et al., 2010; Louvet-Vallée, 2000) (Figure 4A-B). In addition to their architectural role, ERM proteins have been implicated in the maturation of endosomes and trafficking of EGFR (Chirivino et al., 2011). These results indicate that a pool of NICD2 molecules relocates to an ERM enriched microenvironment upon or immediately after gamma secretase cleavage to generate NICD2.

At the 15 min time point after inhibitor washout, the enrichment of ERM proteins has abated and there is a period when relatively few proteins show an enrichment in labeling greater than two-fold when compared to baseline labeling in the presence of GSI (Figure 4C). This time point is characterized by a mild increase in labeling of motor and cytoskeletal proteins, suggesting that NICD2 is primarily cytoplasmic and diffusing passively to the nucleus. Starting with the 5 - 15 min time window, there is also enrichment of proteins that participate in nuclear import of cargo (Wälde et al., 2012; Yokoyama et al., 1995) (Figure 4D), including the importin-beta subunit KPNB1 (Cautain et al., 2015) and its associated adaptor Importin-7, as well as subunits of importin-alpha (KPNA1, KNPA2, and KPNA6) and the nuclear pore protein RANBP2 (also called Nup358).

NICD2 is nuclear and is associated with active transcription within 2 h

Several proteins exhibited a late labeling pattern with a strong peak enrichment at 2 h (Figure 5A-B). MAML1, a component of Notch transcriptional complexes (Nam et al., 2006; Petcherski & Kimble, 2000; Wu et al., 2000), was the most significantly enriched protein at this time point when compared to the baseline GSI condition (Figure 5A), indicative of NICD2 nuclear entry (Figure 5A). Analysis of the kinetics of MAML1 enrichment showed that increased labeling began at 30 min and was maximal by the 2 h timepoint (Figure 1E).

Strikingly, most of the other proteins showing significant, robust enrichment by 2 h are also implicated in transcription regulation or chromatin modification or remodeling (Figure 5A-B). Hierarchical clustering revealed that the pattern of enrichment seen for MAML1 is shared by other transcriptional regulators, including RAI1, TCF20, and FUBP1 (Figure 5B). Likewise, ARID1A and ARID1B of the SWI/SNF chromatin remodeling complex exhibited the same dynamics of labeling enrichment in this experiment. A similar time course of enrichment was also observed for the proteins FUS and EWSR1, two FET proteins that enter nuclear condensates and can influence transcription, and for several HNRNP proteins implicated in the regulation of splicing (Mittal & Roberts, 2020) (Figure 5B). Together, these data indicate that NICD2 has initiated the induction of a transcriptional response as early as 30 min after GSI washout and that the response is robust within 2 h, consistent with other reports showing that dynamic Notch binding sites in the genome become loaded with NICD and other co-factors within 2 h (Fryer et al., 2004; Fryer et al., 2002; Mittal & Roberts, 2020; Pillidge & Bray, 2019).

In an effort to further refine the temporal sequence of association of nuclear factors with NICD2, we acquired a second proximity labeling dataset focusing on timepoints between 30 min and 4 h after GSI washout (Figures 5C and S6A-B). In this experiment, MAML1, CREBBP/p300, the nuclear factor 1 C-type NFIC, and proteins of the BAF chromatin remodeling complex (Figure 5D-F) show enrichment by the 45 min timepoint, reaching maximum enrichment at the 2 h and 4 h timepoints (see Table S2 for full quantification data of all proteins identified in this dataset). Enrichment of other transcriptional regulators (*e.g.,* RAI1), HNRNPs and FET proteins begins shortly afterwards, at 1 h (Figure 5G), indicative of the presence of NICD2 at loci of active transcription by this timepoint.

DISCUSSION

Here, we performed Notch2-APEX2 time-resolved proximity labeling coupled with quantitative multiplexed proteomics to track the molecular microenvironment of endogenous Notch2 as a function of time after ligand stimulation and washout of a gamma secretase inhibitor. This unbiased approach allowed us to measure dynamic changes in the proteins in proximity to Notch before and after cleavage by gamma secretase, investigate the path and mode of transport of activated Notch2 from the plasma membrane to the nucleus, and define the nuclear microenvironment of NICD2 during transcriptional induction.

Several new mechanistic findings emerged from these studies. First, the enrichment of proteins associated with vesicular transport and endocytosis after ligand exposure in GSI-treated cells suggested that gamma secretase cleavage of Notch2 occurs in an intracellular compartment. This conclusion was supported by additional experiments tracking gamma secretase cleavage activity after washout of inhibitors of ligand-dependent metalloprotease (S2) cleavage in the presence of inhibitors of endocytosis or vesicle acidification, which showed that S2-processed Notch2 must enter an intracellular compartment to be cleaved by gamma secretase. Whereas older studies have reached differing conclusions about whether gamma secretase processes substrates at the plasma membrane (Chyung et al., 2005; Hansson et al., 2005) or in an intracellular compartment (Chapman et al., 2016; Gupta-Rossi et al., 2004; Kobia et al., 2014), our finding that gamma secretase cleavage of Notch2 occurs in an intramembrane compartment agrees with recent proteomics studies investigating APP cleavage using affinity capture of the early endosome-associated protein EEA, in which APP/Aβ cleavage products of gamma secretase accumulate in early/sorting endosomes (Park et al., 2022).

Second, our data suggest that Notch2 molecules transiently pass through a microenvironment enriched in ERM proteins between 2-5 min after GSI washout. These proteins appear to identify a compartment traversed by Notch2 upon or immediately after gamma secretase cleavage to generate NICD2. In comparison, few proteins are enriched at the 15 and 30 min time points, consistent with the idea that NICD2 moves by passive diffusion to the nucleus after gamma secretase cleavage, with a possible preference for migration in proximity to or along actin filaments.

Third, we find that NICD2 enters a nuclear microenvironment enriched in components associated with a transcriptional response as early as 30-45 min after GSI washout and persists through the final 4 h timepoint. This timing of transcriptional induction is consistent with previous

real-time luciferase complementation studies using ectopic Notch1 and RBPJ expression (Ilagan et al., 2011) and with the onset and duration of Notch-induced transcription in fly models and in cancer cells (Castel et al., 2013; Falo-Sanjuan & Bray, 2022; Housden et al., 2013; Wang et al., 2014). In addition to MAML1, the nuclear proteins most rapidly recruited to NICD2 are CREBBP/p300, a well-established partner of MAML1 in NICD-dependent transcriptional induction (Fryer et al., 2004; Fryer et al., 2002; Oswald et al., 2001; Wallberg et al., 2002), and components of the BAF chromatin remodeling complex. Strikingly, the SWI/SNF chromatin remodeling complex is crucial to render enhancers responsive to Notch in *Drosophila* (Pillidge & Bray, 2019); the basis for recruitment of the BAF complex to Notch-responsive elements should be fertile ground for future study.

Together, our proximity labeling studies and follow-up cellular assays serve as the basis for a well-defined spatiotemporal model of the pathway traversed by Notch upon proteolytic activation (Figure 6). Ligand engagement first induces S2 cleavage of Notch at the cell surface, followed by entry of truncated Notch2 into an endocytic compartment for cleavage by gamma secretase. As early as 30 min after gamma secretase cleavage, NICD enters the nucleus and by 45 min has begun to recruit CREBBP/p300 and chromatin remodeling complexes to initiate transcription of responsive genes, with evidence for recruitment of proteins involved in transcription-coupled splicing events after 60 – 90 min. More broadly, our work with Notch as a signaling protein of interest represents a proof-of-concept for future quantitative analyses of other signal transduction systems, showing that time-resolved proximity labeling with APEX2 combined with multiplexed proteomics can elucidate the temporal and spatial dynamics of endogenous proteins and the evolution of their microenvironments during signaling.

MATERIALS & METHODS

Key Resources Table

Reagent type	Designation	Source of reference	Identifiers	Additional information
Antibody	Mouse monoclonal anti β-Tubulin (clone D3U1W)	Cell Signaling Technology	RRID: AB_2715541 / Catalog: #86298S	Western blot (1:2000)
Antibody	Rabbit monoclonal anti GAPDH (clone 14C10)	Cell Signaling Technology	RRID: AB_561053 / Catalog: #2118S	Western blot (1:2000)
Antibody	Rabbit monoclonal anti Notch2 (clone D76A6)	Cell Signaling Technology	RRID: AB_10693319 / Catalog: #5732S	Western blot (1:1000)
Antibody	Rabbit anti NICD2	Eli Lilly	(Shanmugam et al., 2021)	Western blot (1:1000) & Immunofluorescence (1:2500)
Antibody	Rabbit monoclonal anti NICD1 (clone D3B8)	Cell Signaling Technology	RRID: AB_2153348 / Catalog: #4147S	Western blot (1:1000)
Antibody	Mouse monoclonal anti HA-tag (clone 6E2)	Cell Signaling Technology	RRID: AB_10691311 / Catalog: #2367S	Western blot (1:500)
Antibody	Rabbit monoclonal anti RBPJ (clone D10A4)	Cell Signaling Technology	RRID: AB_2665555 / Catalog: #5313S	Western blot (1:1000)
Antibody	Mouse monoclonal anti mNEONgreen (clone 6G6)	Chromotek	RRID: AB_2827566 / Catalog: #32F6	Western blot (1:500)
Antibody	Alexa Fluor Plus 647-conjugated donkey anti-rabbit polyclonal secondary	ThermoFisher Scientific	RRID: AB_2762835 / Catalog: #A32795	Immunofluorescence (1:1000)

Cell line	SVG-A	Walter J. Atwood, Brown University	RRID: CVCL_5G13	
Cell line	Notch2 knockout SVG-A cell line	This study		
Cell line	Notch2-APEX2 knockin SVG-A cell line	This study		
Cell line	293T	ATCC	RRID: CVCL_0063 / Catalog: #CRL-3216	
Cell line	U2OS	ATCC	RRID: CVCL_0042 / Catalog: #HTB-96	
Cell line	HeLa	ATCC	RRID: CVCL_0030 / Catalog: #CCL-2	
Cell line	U251	Sigma	RRID: CVCL_0021 / Catalog: #1610381	
Reagent	Biotin-Phenol	Iris Biotech	Catalog: #LS-3500	
Reagent	Hydrogen Peroxide	Sigma	Catalog: #H1009-5ML	
Reagent	Pierce Streptavidin magnetic beads	ThermoFisher Scientific	Catalog: #88817	
Reagent	Streptactin-HRP	Bio-rad	Catalog: #1610381	Western blot (1:1000)
Reagent	JaneliaFluorX549 HaloTag ligand	Luke Lavis, Janelia Research Campus		HaloTag labeling (100 nM)

Cell line generation, cultivation, and manipulation

All cell lines were maintained in DMEM with L-glutamine (Corning) supplemented with 10% fetal bovine serum (FBS, Gemini Bio-Sciences) and 1% penicillin-streptomycin (Gibco) at 37°C and 5% CO_2. Cell lines were tested for mycoplasma on a regular basis. CRISPR/Cas9 gene editing was used to knock out Notch2 in SVG-A cells. For the SVG-A Notch2 knockout cell line, a pX459 plasmid containing a gene-specific guide RNA (gRNA) was transfected using Lipofectamine 2000 (ThermoFisher Scientific) according to the manufacturer's instructions (see Table S3 for gRNA sequences used in this study). 48 h after transfection, cells were selected using 2 µg/mL puromycin for 3 days, and single cells were then isolated by flow cytometry using a BD FACSAria cell sorter.

Knockout clones were identified by DNA sequencing after PCR amplification of genomic DNA at the mutated locus, and the loss of protein expression was confirmed by Western blotting.

CRISPR/Cas9 genome editing was also used to fuse an APEX2-HA tag at the C-terminus of endogenous Notch2 in SVG-A cells. SVG-A cells were co-transfected with a pX459 plasmid containing gRNA targeting Notch2 (see Table S3 for gRNA sequences) and a pUC19 donor plasmid containing a GGAG linker-APEX2-HA-T2A-mNEONGreen cassette flanked by Notch2 genomic locus homology arms each approximately one kilobase in length. Seven days after transfection, single cells expressing mNEONGreen were isolated by FACS using a Sony SH800S cell sorter, and individual clones were expanded in 96 well plates. Confirmation of successful tagging and identification of homozygous clones was carried out by PCR amplifying the region of the insertion with flanking primers outside of the genomic region covered by the homology arms, followed by Sanger DNA sequencing for the positive homozygous clones. Clones were further evaluated to assess the amount of expressed Notch2 protein by Western blotting, the amount of surface staining by flow cytometry on a BD Accuri C6 Plus flow cytometer, Notch2 transcriptional activity using a luciferase reporter assay (described below), and APEX2-dependent protein biotinylation by Western blotting using Streptactin-HRP (Bio-Rad). A similar strategy and gRNA were used to insert a HaloTag at the C-terminus of endogenous Notch2.

Western blotting

Adherent cells were washed in ice-cold Dulbecco's Phosphate Buffered Saline (DPBS) and lysed in gel-loading buffer (2% SDS, 60 mM Tris–HCl pH 6.8, 100 mM DTT, 10% glycerol, and 0.005% bromophenol blue), scraped off the plate, boiled at 95°C for 5 minutes, and subjected to SDS-PAGE. Proteins were then transferred to a PROTRAN 0.2 µm nitrocellulose membrane (Cytiva) and stained with Ponceau S (Sigma-Aldrich). Membranes were incubated in 5% (w/v) non-fat dry milk in TBST (20 mM Tris, 150 mM NaCl, 0.2% Tween-20, pH 7.6) at room temperature for at least 1 h. Blocked membranes were incubated with various primary antibodies, or with a Streptactin-HRP (BioRad), diluted in TBST supplemented with 5% non-fat dry milk overnight at 4°C with gentle shaking. Membranes were washed 3 times with TBST at room temperature and incubated with appropriate secondary antibodies for 1 h at room temperature with gentle shaking. Blots were washed 3 times with TBST and imaged using an Odyssey Infrared Imaging System

(LI-COR Biosciences) for IRDye-conjugated secondary antibodies or on a Chemidoc (Bio-Rad) using an Amersham ECL Western Blotting Detection kit (GE Healthcare) for Streptactin-HRP.

Recombinant Jag1-Fc expression and purification

The extracellular domain (ECD) of human Jag1 (aa 1-1067) was fused to the Fc region (CH2 and CH3 domains) and hinge region of the human IgG1 heavy chain in the pFUSE-Fc1 vector (InvivoGen). Jag1ECD-Fc protein was expressed in Expi293F cells grown in Expi293F expression medium at 37°C in an 8% CO_2 incubator with constant shaking. Cells were grown to a density of $3x10^6$ cells/mL in a final volume of 1 L and transiently transfected using FectoPro transfection reagent (Poly-plus) with 1 mg of purified plasmid at a 2:1 DNA/FectoPro ratio. 22 h after transfection, 5 mM Valproic acid sodium salt (Sigma-Aldrich) and 10 mL of 45% D-(+)-Glucose solution (Sigma-Aldrich) were added. After 7 days of culture, the media supernatant was collected after removal of debris by centrifugation at 4,000 xg for 15 min at 4°C followed by a filtration step. Filtered media was then loaded onto a Protein A (Millipore) column prewashed in ice cold HEPES-buffered saline (HBS) buffer (20 mM HEPES pH 7.3, 150 mM NaCl). Bound protein was eluted in 100 mM glycine, pH 3.0 and neutralized with 1 M Tris buffer pH 7.3. Eluted protein was buffer exchanged and concentrated in HBS. Protein purity was assessed by separation on SDS-PAGE after staining with SafeBlue (ThermoFisher Scientific). The purified protein was diluted to a final concentration of 200 µg/mL in HBS supplemented with 10% glycerol, aliquoted, flash frozen, and stored at -80°C.

Activation of Notch2 by immobilized Jag1-Fc

Recombinant Jag1-Fc was immobilized by overnight incubation at 4°C in individual wells of non-tissue culture-treated 6 or 12 well plates (VWR) at a final concentration of 2 µg/mL in DPBS containing 10 µg/mL poly-D-lysine (ThermoFisher Scientific). For imaging studies, the ligand was immobilized in 24 well plates containing pre-washed glass coverslips overnight. The next day, the Jag1-Fc and poly-D-lysine mixture was removed and the cells were added to the coverslips and incubated as indicated.

Drug treatments and washouts

For GSI or GI254023X washout experiments, cells were recovered by centrifugation, resuspended and washed three times with the appropriate culture media, and then incubated in fresh media at 37°C for the indicated time. For experiments using hydroxy-dynasore, bafilomycinA1, or chloroquine, cells were incubated in the presence of GSI (Compound E, EMD Millipore) or GI254023X (Sigma-Aldrich) overnight, and were pre-incubated with the indicated inhibitor 1 h before removing the GSI or GI254023X. Cells were then incubated in the continued presence of hydroxy-dynasore (Sigma-Aldrich), bafilomycinA1 (Selleck Chemicals), or chloroquine (Sigma-Aldrich), at 37°C for the indicated time. Hydroxy-dynasore incubation was performed in serum-free DMEM.

Luciferase reporter assays

SVG-A cells were transfected with a mixture of TP1-firefly luciferase and pRL-TK (Promega) plasmids at a 49:1 ratio using Lipofectamine 2000 (ThermoFisher Scientific) according to the manufacturer's instructions. Culture media was replaced 4 h after transfection and the cells were incubated overnight. The next day, cells were detached with 0.5 mM EDTA, recovered by centrifugation, and added to plates pre-coated with recombinant Jag1-Fc in media containing 100 nM Compound E (GSI) or 5 μM GI254023X. At that time, luciferase assays were performed using a Dual-Luciferase reporter assay system (Promega) according to the manufacturer's instructions. For experiments investigating the effects of endocytosis or vesicular acidification, cells were preincubated with hydroxy-dynasore, bafilomycinA1, or chloroquine for 1 h before removal of GI254023X, and cells were harvested 6 hours later. Luminescence was measured on a GloMax plate reader (Promega). Three technical measurements were performed for each of three biological replicates. The ratio of firefly to Renilla luminescence was calculated and normalized to the control condition (presence of GI254023X and DMSO) and assigned a value of 100 percent.

APEX2 proximity labeling

SVG-A Notch2-APEX2-HA cells were incubated in media supplemented with 2 mM biotin phenol (BP, Iris Biotech Gmbh, LS-3500) for 1 h before adding hydrogen peroxide (H_2O_2, Sigma-Aldrich) to a final concentration of 0.1 mM. 30% (v/v) H_2O_2 stock solution was freshly diluted to 1 M in DPBS immediately before each experiment. Washouts of GSI were performed so that each sample was incubated for exactly 1 h with BP prior to H_2O_2 exposure. Immediately after adding H_2O_2, the

441 culture dishes were gently rocked several times to ensure optimal H_2O_2 distribution. Exactly 1 min
442 after the addition of H_2O_2, the media was quickly aspirated and cells were washed three times with
443 quenching buffer (DPBS supplemented with 10 mM sodium ascorbate, 5 mM Trolox [Sigma-
444 Aldrich], and 10 mM sodium azide). Cells were then scraped in quenching buffer, harvested by
445 centrifugation, and cell pellets were flash-frozen and stored at -80°C until streptavidin pull-down
446 was performed.
447
448 **Streptavidin pull-down**
449 All solutions and buffers were freshly prepared and filtered. Streptavidin capture of biotinylated
450 proteins was performed as previously described (Kalocsay, 2019; May et al., 2021). Briefly, frozen
451 cell pellets were lysed in ice cold lysis buffer (8 M Urea, 100 mM sodium phosphate pH 8.0, 1%
452 SDS (w/v), 100 mM NH_4HCO_3, 10 mM TCEP) and pipetted repeatedly on ice to ensure proper
453 cell lysis. Lysates were then homogenized by passing them through QIAshredder cartridges
454 (Qiagen). Proteins were precipitated by adding an equal volume of ice cold 55% Trichloroacetic
455 acid (TCA, Sigma-Aldrich), incubated 15 min on ice, and then pelleted by centrifugation at 21,000
456 x g at 4°C for 10 min. The protein pellet was washed with -20°C cold acetone (Sigma-Aldrich),
457 vortexed, and centrifuged at 21,000 x g at 4°C for 10 min. Following centrifugation, acetone was
458 removed and the pellet was washed with acetone 3 more times. After the last wash, the pellet was
459 resuspended in lysis buffer as described above, vortexed, and rotated at room temperature until
460 fully dissolved, allowing reduction of proteins by TCEP at the same time.
461 Resuspended proteins were centrifuged at 21,000 x g at room temperature for 10 min and
462 the clear supernatant was transferred to a new microcentrifuge tube. To alkylate free cysteines,
463 freshly prepared 400 mM iodoacetamide stock solution (Sigma-Aldrich) in 50 mM ammonium
464 bicarbonate was added to the supernatant at a final concentration of 20 mM, and the samples were
465 immediately vortexed and then incubated in the dark at room temperature for 25 min. After
466 alkylation, freshly prepared dithiothreitol (DTT, Sigma-Aldrich) was added to a final
467 concentration of 50 mM to quench the reaction. Finally, water was added to each sample to reach
468 a final concentration of 4 M urea and 0.5% (w/v) of SDS.
469 125 µL of streptavidin magnetic bead suspension (ThermoFisher Scientific) was washed
470 twice with 4 M urea, 0.5% SDS (w/v), 100 mM sodium phosphate pH 8.0 and added to each
471 sample. The tubes were gently rotated overnight at 4°C. Following capture of biotinylated proteins,

the magnetic beads were washed 3 times with 4 M urea, 0.5% SDS (w/v), 100 mM sodium phosphate pH 8.0, 3 more times with the same buffer without SDS, and finally 3 more times with DPBS. The beads were transferred to new tubes for each change of wash buffer.

On-beads digestion and tandem mass tag (TMT) labeling

The streptavidin beads were subjected to on-bead protease digestion in 50 µl digestion buffer (200 mM EPPS pH 8.5 with 2% acetonitrile [v/v]) along with LysC (Wako) at an enzyme-to-substrate ratio of 1:50. The samples were incubated at 37°C for 3 h. Then 50 µl of digestion buffer with trypsin (Promega) was added at an enzyme-to-substrate ratio of 1:100. The digestion was continued at 37˚C overnight with gentle agitation. The clear supernatants of digested protein were separated from beads with a magnetic rack and transferred to fresh tubes.

For the TMT reaction, 30% acetonitrile (v/v) was added to the digested protein and then labeled using a TMT isobaric mass tagging kit (ThermoFisher Scientific). The TMT reaction was performed for 1 h according to the manufacturer's instructions. TMT labeling efficiency and ratios were measured by LC-MS3 analysis after combining equal volumes from each sample. Once the labeling efficiency was determined to be >95%, the TMT reactions were quenched with hydroxylamine 0.5% v/v for 15 min and acidified with formic acid. Samples were then pooled and dried to near completion under reduced pressure before resuspension in 1% formic acid and fractionation using a Pierce High pH Reversed Phase Peptide Fractionation Kit (ThermoFisher Scientific) with modified elution of 12 sequential fractions (10%, 12.5%, 15%, 17.5%, 20%, 25%, 30%, 35%, 40%, 50%, 65% and 80% acetonitrile). Fractions were then combined into pairs as follows, 1+7, 2+8, 3+9, 4+10, 5+11, 6+12, to give the final six fractionated samples. The resulting fractions were dried under reduced pressure and then desalted using a stage tip protocol (Rappsilber et al., 2007).

Mass spectrometry acquisition and data analysis

Data were acquired on an Orbitrap Fusion Lumos instrument (ThermoFisher Scientific) coupled to a Proxeon Easy-nLC 1200 UHPLC. Peptides were injected onto a 100 µm (inner diameter) capillary column (~30 cm) packed in-house with C18 resin (2.6 µm, 150Å, ThermoFisher Scientific). Peptide fractions were separated with a 4 h acidic acetonitrile gradient from 5-35% Buffer B (Buffer A = 0.125% formic acid, Buffer B = 95% acetonitrile, 0.125% formic

acid). All data were collected with a multi notch MS3 method (McAlister et al., 2014). MS1 scans (Orbitrap analysis; resolution 120,000; mass range 400–1400 Th) were followed by MS2 analysis with collision-induced dissociation (CID, CE=35) and a maximum ion injection time of up to 120 ms and an isolation window of 0.4 m/z, using rapid scan mode. To obtain quantitative information, MS3 precursors were fragmented by high-energy collision-induced dissociation (HCD, CE=65) and analyzed in the Orbitrap at a resolution of 50,000 at 200 Th with max injection time set to 650 ms. Raw spectra were converted to mzXML to correct monoisotopic m/z measurements and to perform a post-search calibration.

Spectra were searched using SEQUEST (v.28, rev.12) software against the UniProt human reference proteome (downloaded 02-25-2020), containing common contaminants and reversed order protein sequences as decoy hits (Eng et al., 1994). Searches were performed with a precursor mass tolerance of 20 ppm, and the fragment-ion tolerance was set to 0.9 Da. For searches a maximum of 2 missed trypsin cleavage sites were allowed. Oxidized methionines (+15.9949 Da) were set as a variable modification, while cysteine carboxyamidomethylation (+57.0215) and TMT (+229.1629 or TMT16 (+304.2071 Da) tags on lysine and peptide N-termini were set as a static modification. Peptide spectral matches (PSM) were filtered by linear discriminant analysis (LDA), using a target-decoy database search to adjust the PSM false discovery rate to 1% and protein level FDR of 1% (Huttlin et al., 2010). For MS3 relative quantification, peptides were filtered for an MS2 isolation specificity of >70%, and a total TMT summed signal to noise of >200 for all channels in the multiplex. Further details of the TMT quantification method and search parameters applied were described previously (Paulo et al., 2016).

Proteomics raw data and search results were deposited in the PRIDE archive for each multiplex experiment with accession number: PXD039008 (immobilized ligand with GSI experiment, Table S1) and PXD039010 (immobilized ligand with GSI nuclear centered experiment, Table S2).

Immunofluorescence and image processing

SVG-A Notch2-HaloTag cells were grown on ligand-coated coverslips. Cells were labeled with JaneliaFluorX549 HaloTag ligand (a gift from Luke Lavis, Janelia Research Campus) at a final concentration of 100 nM in media for 15 min at 37°C. The media was then removed, cells washed with fresh media, and returned to the incubator for 1 h to allow newly synthesized labeled

Notch2 to be delivered to the plasma membrane. Cells were treated with the indicated vesicular/transport inhibitors prior to GI254023X/GSI washout, as described above.

2 h after washout of GI254023X or GSI, cells were washed 3 times in DPBS, fixed with 4% paraformaldehyde (PFA, Sigma-Aldrich) for 15 min at room temperature (RT), washed three times in DPBS, and quenched with 0.1 M Glycine pH 7.5 in DPBS for 15 min at RT. After another three PBS washes, fixed cells were permeabilized with 0.1% Triton X-100 in DPBS for 10 min at room temperature followed by three washes in DPBS and blocking in 5% BSA (w/v) in DPBS for 1 hour at room temperature. Cells were then incubated for 1 h with primary antibodies diluted in blocking buffer at room temperature. After three washes in DPBS, the cells were incubated with secondary antibody (Alexa Fluor Plus 647-conjugated anti-rabbit, ThermoFisher Scientific A32795) diluted in blocking buffer for 45 min at room temperature followed by three washes in DPBS. For DNA staining, cells were incubated with SYTOX Green Nucleic Acid Stain (ThermoFisher Scientific) according to manufacturer's recommendations followed by three washes in DPBS. Coverslips were then mounted with ProLong Gold Antifade Mountant with DAPI (ThermoFisher Scientific) or without DAPI if already labeled with SYTOX Green. Coverslips were stored at 4°C before image acquisition.

Images were acquired using a Marianas system (Intelligent Imaging Innovation) composed of a Zeiss Axio-Observer Z1 (Carl Zeiss) equipped with a 63x objective (Plan-Apochromat, NA 1.4, Carl Zeiss), a spinning disk confocal head (CSU-XI, Yokogawa Electric Corporation) and a spherical aberration correction system (Infinity Photo-Optical). Excitation light was provided by 405, 488, 561, or 640 nm solid-state lasers (Sapphire, 50 mW, Coherent Inc) coupled to an acoustic-optical tunable filter. Laser power and exposure times were kept the same for all experiments. Z stacks of 38 x-y confocal images were obtained in 270 nm z-steps using a cooled CCD camera (QuantEM, 512SC, Photometrics). All equipment was controlled by SlideBook acquisition software (Intelligent Imaging Innovations).

Image processing was performed using Fiji software (Schindelin et al., 2012). For nuclear intensity measurements, the nucleus was identified by DAPI or SYTOX Green staining and the mean fluorescence of each indicated channel was measured by applying a nucleus mask. After removing the raw nuclear background for each channel, the mean fluorescence intensity was normalized to a control condition assigned a value of 100 percent.

Statistical analysis

Statistical analyses of fluorescence microscopy, luciferase reporter assays, qPCR, and Western blotting experiments were performed using GraphPad Prism software (GraphPad). One-way ANOVA testing was performed for the comparison of multiple groups. All error bars denote mean ± standard deviation. *$p < 0.05$, **$p < 0.01$, ***$p < 0.001$. The number of individual experiments analyzed is indicated in the figure legends.

ACKNOWLEDGMENTS

We thank members of the Blacklow lab for helpful discussions. This work was supported by NIH awards 1R35 CA220340 and R01 CA272484 (to S.C.B. and T.K.), 5R35 GM130386 (to T.K.), and K99 GM144750 (to J.M.R.). A.P.M was supported by a Merck Postdoctoral Fellowship. J.C.A. is supported by the Ludwig Center at Harvard.

AUTHOR CONTRIBUTIONS

A.P.M. and S.C.B. conceived the project. S.C.B. and T.K. acquired funding. A.P.M. performed and analyzed experiments. E.D.E. performed initial characterization of the parental SVG-A cell line and designed and generated Notch2-HaloTag knockin and Notch2 knockout lines. G.A.B., R.J.E., and M.K., processed and analyzed mass spectrometry data. L.T., G.S., and T.K., assisted with and gave technical advice for microscopy experiments. J.M.R., J.C.A., A.N.D., and M.K. assisted with data analysis and interpretation. A.P.M. and S.C.B. wrote the manuscript with input from all authors. All authors provided feedback and agreed on the final manuscript.

DECLARATION OF INTERESTS

S.C.B. is on the board of directors of the non-profit Institute for Protein Innovation and the Revson Foundation, is on the scientific advisory board for and receives funding from Erasca, Inc. for an unrelated project, is an advisor to MPM Capital, and is a consultant for IFM, Scorpion Therapeutics, Odyssey Therapeutics, Droia Ventures, and Ayala Pharmaceuticals for unrelated projects. J.C.A. is a consultant for Ayala Pharmaceuticals, Cellestia, Inc., SpringWorks Therapeutics, and Remix Therapeutics.

FIGURE LEGENDS

Figure 1: Design, experimental procedure, and overall kinetic profiles of time-resolved Notch2-APEX2 proximity labeling in SVG-A cells. (A) Schematic of key steps in Notch2 signaling induced by immobilized Jag1 ligand. Jag1 stimulates Notch2 proteolysis at S2 by ADAM10, followed by gamma secretase cleavage at S3. The S3-cleaved Notch2 intracellular domain (NICD2) transits to the nucleus and associates with RBPJ and the transcriptional co-activator MAML1 to induce the expression of target genes. BB94 and GI254023X (also referred as GI25X) are inhibitors of ADAM10, and Compound E (referred to as GSI) is a potent inhibitor of gamma secretase. (B) Schematic showing the design for time-resolved proximity labeling by Notch2-APEX2 using plated Jag1 as ligand and washout of GSI at time t=0. (C) Heatmap of hierarchical clustering of Notch2-APEX2 proximity labeling as a function of time after washout. Clustering of the relative abundance of each identified protein (columns) as a function of time (rows) was performed using Ward's minimum variance method. Color palette representing the relative abundance for each protein (minimum to maximum) is shown on the right. (D-F) Kinetic profiles of representative proteins showing an early (D), late (E), or sustained (F) labeling pattern.

Figure 2: Changes in the Notch2 microenvironment upon stimulation by ligand in the presence of GSI. (A) Heatmap of hierarchical clustering of proteins characterized by peak relative abundance in conditions without Notch stimulation by ligand. (B) Gene Ontology terms for proteins significantly enriched in panel A. (C) Volcano plot comparing relative abundance of proteins enriched upon Jag1 stimulation in GSI compared to no ligand stimulation. Significantly enriched proteins (p-value ≤ 0.05, FC ≥ 1.5) related to endocytosis and/or vesicular-mediated transport are labeled in orange, whereas significantly downregulated proteins that localize to the

plasma membrane are labeled in green. P-values are Benjamini-Hochberg corrected. (D) Heatmap focused on proteins related to endocytosis and vesicular transport identified in the time-resolved Notch2-APEX2 proximity labeling analysis. (E) Gene Ontology terms for proteins significantly enriched in panels C and D.

Figure 3: Effects of acidification and endocytosis inhibitors on Notch2 activity after removal of ADAM10 or gamma secretase inhibitors. (A) Representative images of Jag1-stimulated SVG-A Notch2-HaloTag cells showing the cellular distribution of Notch2-HaloTag (Notch2-Halo) and (S3-cleaved) NICD2 after removal of the ADAM10 inhibitor GI254023X in the absence or presence of hydroxy-dynasore (20 μM), bafilomycinA1 (BafA1; 25 nM), or chloroquine (50 μM). The HaloTag was labeled with JaneliaFluorX549 HaloTag ligand and NICD2 was stained with an anti-NICD2 primary antibody and anti-rabbit secondary antibody conjugated to Alexa Fluor 647. Nuclei were identified by DAPI staining. Scale bars: 20 μm. (B-C) Quantification of signal intensity in the nucleus for Notch2-Halo (B) and for NICD2 (C) for the imaging data presented in panel A. (D) Quantification of Western blot data for NICD2 abundance after GI254023X washout in the presence of hydroxy-dynasore (20 μM), bafilomycinA1 (BafA1; 25 nM), or chloroquine (50 μM). (E) Representative Western blot for NICD2 quantified in panel D (see Supplemental Figure 5 for NICD1 and NICD2 generation in other cell lines). (F) Notch luciferase reporter assay. Parental SVG-A cells were stimulated by immobilized Jag1 overnight in the presence of GI254023X, and the relative luciferase activity was measured 6 h after removal of the ADAM10 inhibitor GI254023X in the absence or presence of hydroxy-dynasore (20 μM), bafilomycinA1 (BafA1; 25 nM), or chloroquine (50 μM). (G-H) Quantification of signal intensity in the nucleus (see Supplemental Figure 4B for imaging data) for Notch2-Halo (G) and activated

NICD2 (H) after removal of the GSI compound E (100 nM) in the absence or presence of hydroxy-dynasore (20 μM), bafilomycinA1 (BafA1; 25 nM), or chloroquine (50 μM). All data presented in this figure are from three biological replicates.

Figure 4: NICD2 microenvironment early after GSI washout. (A) Hierarchical clustering of the proteins characterized by a peak of relative abundance between 2 - 5 min after GSI removal, focusing on neighbors closest to Ezrin (EZR). (B,C) Volcano plots comparing Notch2 proximity-labeled proteins enriched at the 5 (B) and 15 (C) min timepoints after GSI removal when compared to GSI (t=0). Proteins related to actin, myosin, or cytoskeletal transport are labeled in blue, and proteins related to endocytosis or vesicular-mediated transport are labeled in orange. P-values are Benjamini-Hochberg corrected (p-value ≤ 0.05, FC ≥ 1.5). (D) Heatmap showing the enrichment pattern of proteins related to nuclear import identified by Notch2 proximity labeling.

Figure 5: Nuclear accumulation of NICD2 and engagement with transcriptional regulators (A) Volcano plot highlighting Notch2 proximity-labeled proteins enriched 2 h after GSI removal when compared to GSI (t=0). Significantly enriched proteins (p-value ≤ 0.05, FC ≥ 1.5) implicated in transcriptional activity are red, and other nuclear proteins are indicated in yellow. P-values are Benjamini-Hochberg corrected. (B) Heatmap showing kinetic profiles of proteins that cluster adjacent to MAML1 with strong enrichment 2 h after GSI washout. (C) Schematic showing the design for focused proximity labeling around the time of NICD2 nuclear entry using plated Jag1 as ligand and washout of GSI at time t=0 (see Supplemental Figure 6). (D) Heatmap of hierarchical clustering centered on proteins with kinetic profiles most closely related to MAML1 in the nuclear-centered proximity labeling dataset (see Supplemental Figure 6). (E) Volcano plot of Notch2

proximity-labeled proteins enriched 45 min after GSI removal when compared to GSI (t=0) in the nuclear-centered dataset. Significantly enriched proteins (p-value ≤ 0.05, FC ≥ 1.5) implicated in transcriptional activity are red. P-values are Benjamini-Hochberg corrected. (F) Line plots showing the kinetic profiles of MAML1, the SWI/SNF chromatin-remodeling complex component ARID1A, CREBBP/p300, and the nuclear factor 1 C-type (NFIC) and (G) line plots showing the kinetic profiles of the transcriptional regulators EWSR1, RAI1, KHSRP, and TAF15 in the nuclear-centered dataset.

Figure 6: Model including Notch2 internalization as a mechanistic step in Notch activation and signaling. Upon ligand stimulation of SVG-A cells, Notch2 is cleaved at site S2 by ADAM10, followed by entry of S2 processed Notch2 molecules into an intracellular compartment. Internalized Notch2 molecules are then cleaved at site S3 by gamma secretase, generating NICD2, which access the nucleus about 30-45 min after GSI washout and induces its transcriptional response.

Supplemental Figure 1: SVG-A Notch2-APEX2 cell line validation, related to Figure 1. (A) Western blot probing for Notch2 in lysates from parental and Notch2 knockout SVG-A cells. (B) Notch luciferase reporter assay, measuring relative luciferase activity in parental or Notch2 knockout SVG-A cells cultured with or without immobilized Jag1. (C) Design strategy for CRISPR/Cas9-mediated Notch2-APEX2 knock-in in SVG-A cells. An APEX2-HA-T2A-mNEONgreen cassette was inserted at the C-terminus of the genomic locus of the *NOTCH2* gene. The addition of the T2A-mNEONgreen enabled fluorescence-activated cell sorting (FACS) of clones with genomic integration of the repair template. (D) Western blot probing for Notch2 in

lysates from parental and Notch2-APEX2 knock-in cells. (E) Notch luciferase reporter assay, measuring relative luciferase activity in parental or Notch2 knockout SVG-A cells cultured with or without immobilized Jag1 in the presence of DMSO carrier, 100 nM GSI, or 10 μM BB94. (F) Streptactin blot of parental and Notch2-APEX2 SVG-A cells probing biotinylation as a function of added biotin-phenol, H_2O_2, or both molecules.

Supplemental Figure 2: Notch2-APEX2 activation kinetics and biotinylation patterns, related to Figure 1. (A) Western blot of Jag1-stimulated SVG-A cell lysates, probing for activated NICD2 as a function of time after removal of GSI (100 nM). (B) Streptactin blot of Jag1-stimulated SVG-A cell lysates, probing for proteins biotinylated by Notch2-APEX2 as a function of time after removal of GSI (WO).

Supplemental Figure 3: Notch2-APEX2 proximity labeling workflow and time-course reproducibility, related to Figure 1. (A) Sample preparation and mass spectrometry workflow for analysis of the Notch2-APEX2 proximity labeling time course. After collection, samples were lysed and biotin-labeled proteins were purified by streptavidin pull-down in denaturing conditions. Recovered proteins were digested with trypsin, and then labeled using tandem mass tags (TMT, 16 plex) to enable quantitative mass spectrometric analysis of 16 different samples at the same time. (B) Pearson correlation matrix showing good reproducibility between internal replicates. (C) Principal Component Analysis (PCA) of the Notch2-APEX2 proximity labeling time-course. Each dot represents a sample and each color a time point. (D) Western blots of Jag1-stimulated Notch2-APEX2 knock-in SVG-A cells, probing for RBPJ as a function of time after GSI washout. Top: input; bottom: streptavidin pull-down.

Supplemental Figure 4: Effect of inhibition of endocytosis or vesicular acidification on NICD2 nuclear accumulation after GI254023X or GSI washout, related to Figure 3. (A) Representative images of SVG-A Notch2-HaloTag cells showing the subcellular localization of Notch2-HaloTag (Notch2-Halo) and (S3-cleaved) NICD2 in the presence of DMSO, 5 µM GI254023X, 100 nM GSI, 20 µM hydroxy-dynasore, 25 nM bafilomycinA1 (BafA1), or 50 µM chloroquine in the absence of ligand stimulation. The HaloTag was labeled with JaneliaFluorX549 HaloTag ligand and NICD2 was stained with an anti-NICD2 primary antibody and anti-rabbit secondary antibody conjugated to Alexa Fluor 647. Nuclei were identified by DAPI staining. Scale bars: 20 µm. (B) Representative images of Jag1-stimulated SVG-A-Notch2-HaloTag cells showing the subcellular localization of Notch2-HaloTag (Notch2-Halo) and (S3-cleaved) NICD2 before and after removal of GSI (100 nM) in the absence or presence of hydroxy-dynasore (20 µM), bafilomycinA1 (BafA1; 25 nM), or chloroquine (50 µM). Nuclei were identified by DAPI staining. Scale bars: 20 µm.

Supplemental Figure 5: Effect of inhibition of endocytosis or vesicular acidification on NICD1 and NICD2 generation in different cell lines, related to Figure 3. (A-E) Representative Western blot analysis (left) and quantifications (right) for NICD1 and/or NICD2 in Jag1-stimulated SVG-A (A), 293T (B), U2OS (C), HeLa (D) , or U251 (E) cells 2 h after GI25X washout in the presence of different endocytosis and vesicular trafficking inhibitors. All quantifications presented in this figure are from 3 biological replicates.

Supplemental Figure 6: Notch2-APEX2 time-resolved proximity labeling focused on nuclear entry, related to Figure 5. (A) Principal Component Analysis (PCA) of enrichment profiles of the proteins identified in the Notch2-APEX2 proximity labeling time-course centered around NICD2 nuclear entry. Each dot represents a sample and each color a time point. (B) Heatmap of hierarchical clustering of Notch2-APEX2 proximity labeling as a function of time after GSI washout using plated Jag1 with timepoints centered around NICD2 nuclear entry. Clustering of the relative abundance of each identified protein (columns) as a function of time (rows) was performed based on Ward's minimum variance method. The color scheme representing the relative abundance for each protein (minimum to maximum) is shown on the right.

Supplemental Table S1: List of proteins identified and their enrichment levels for Notch2-APEX2 using immobilized ligand with GSI washout.

Supplemental Table S2: List of proteins identified and their enrichment levels for Notch2-APEX2 using immobilized ligand with GSI nuclear centered washout.

Supplemental Table S3: List and sequence of primers used in this study.

REFERENCES

Aber, R., Chan, W., Mugisha, S., & Jerome-Majewska, L. A. (2019). Transmembrane emp24 domain proteins in development and disease. In *Genetics Research* (Vol. 101). Cambridge University Press. https://doi.org/10.1017/S0016672319000090

Aster, J. C., Pear, W. S., & Blacklow, S. C. (2016). The Varied Roles of Notch in Cancer. *Annual Review of Pathology: Mechanisms of Disease*, *12*(1), 245–275. https://doi.org/10.1146/annurev-pathol-052016-100127

Aster, J. C., Xu, L., Karnell, F. G., Patriub, V., Pui, J. C., & Pear, W. S. (2000). Essential Roles for Ankyrin Repeat and Transactivation Domains in Induction of T-Cell Leukemia by Notch1. *Molecular and Cellular Biology*, *20*(20), 7505–7515. https://doi.org/10.1128/mcb.20.20.7505-7515.2000

Bailis, W., Yashiro-Ohtani, Y., & Pear, W. S. (2014). Identifying direct Notch transcriptional targets using the GSI-washout assay. *Methods in Molecular Biology (Clifton, N.J.)*, *1187*, 247–254. https://doi.org/10.1007/978-1-4939-1139-4_19

Castel, D., Mourikis, P., Bartels, S. J. J., Brinkman, A. B., Tajbakhsh, S., & Stunnenberg, H. G. (2013). Dynamic binding of RBPJ is determined by Notch signaling status. *Genes & Development*, *27*(9), 1059–1071. https://doi.org/10.1101/GAD.211912.112

Cautain, B., Hill, R., de Pedro, N., & Link, W. (2015). Components and regulation of nuclear transport processes. In *FEBS Journal* (Vol. 282, Issue 3, pp. 445–462). Blackwell Publishing Ltd. https://doi.org/10.1111/febs.13163

Chapman, G., Major, J. A., Iyer, K., James, A. C., Pursglove, S. E., Moreau, J. L. M., & Dunwoodie, S. L. (2016). Notch1 endocytosis is induced by ligand and is required for signal transduction. *Biochimica et Biophysica Acta - Molecular Cell Research*, *1863*(1), 166–177. https://doi.org/10.1016/j.bbamcr.2015.10.021

Chirivino, D., del Maestro, L., Formstecher, E., Hupé, P., Raposo, G., Louvard, D., & Arpin, M. (2011). The ERM proteins interact with the HOPS complex to regulate the maturation of endosomes. *Molecular Biology of the Cell*, *22*(3), 375–385. https://doi.org/10.1091/mbc.E10-09-0796

Chow, V. W., Mattson, M. P., Wong, P. C., & Gleichmann, M. (2010). An overview of APP processing enzymes and products. In *Neuromolecular medicine* (Vol. 12, Issue 1, pp. 1–12). NIH Public Access. https://doi.org/10.1007/s12017-009-8104-z

Christy J. Fryer, J. Brandon White, & Katherine A. Jones. (2004). Mastermind Recruits CycC:CDK8 to Phosphorylate the Notch ICD and Coordinate Activation with Turnover. *Molecular Cell*, 509–520. https://doi.org/https://doi.org/10.1016/j.molcel.2004.10.014

Chyung, J. H., Raper, D. M., & Selkoe, D. J. (2005). γ-Secretase Exists on the Plasma Membrane as an Intact Complex That Accepts Substrates and Effects Intramembrane Cleavage,. *Journal of Biological Chemistry*, *280*(6), 4383–4392. https://doi.org/10.1074/JBC.M409272200

Delaney, C., Varnum-Finney, B., Aoyama, K., Brashem-Stein, C., & Bernstein, I. D. (2005). Dose-dependent effects of the Notch ligand Delta1 on ex vivo differentiation and in vivo marrow repopulating ability of cord blood cells. *Blood*, *106*(8), 2693. https://doi.org/10.1182/BLOOD-2005-03-1131

Eng, J. K., McCormack, A. L., & Yates, J. R. (1994). An approach to correlate tandem mass spectral data of peptides with amino acid sequences in a protein database. *Journal of the American Society for Mass Spectrometry*, *5*(11), 976–989. https://doi.org/10.1016/1044-0305(94)80016-2

Falo-Sanjuan, J., & Bray, S. J. (2022). Notch-dependent and -independent transcription are modulated by tissue movements at gastrulation. *ELife*, *11*. https://doi.org/10.7554/ELIFE.73656

Fehon, R. G., McClatchey, A. I., & Bretscher, A. (2010). Organizing the cell cortex: The role of ERM proteins. In *Nature Reviews Molecular Cell Biology* (Vol. 11, Issue 4, pp. 276–287). Nat Rev Mol Cell Biol. https://doi.org/10.1038/nrm2866

Fryer, C. J., Lamar, E., Turbachova, I., Kintner, C., & Jones, K. A. (2002). Mastermind mediates chromatin-specific transcription and turnover of the notch enhancer complex. *Genes and Development*, *16*(11), 1397–1411. https://doi.org/10.1101/gad.991602

Gordon, W. R., Zimmerman, B., He, L., Miles, L. J., Huang, J., Tiyanont, K., McArthur, D. G., Aster, J. C., Perrimon, N., Loparo, J. J., & Blacklow, S. C. (2015). Mechanical Allostery: Evidence for a Force Requirement in the Proteolytic Activation of Notch. *Developmental Cell*, *33*(6), 729–736. https://doi.org/10.1016/j.devcel.2015.05.004

Gupta-Rossi, N., Six, E., LeBail, O., Logeat, F., Chastagner, P., Olry, A., Israël, A., & Brou, C. (2004). Monoubiquitination and endocytosis direct γ-secretase cleavage of activated Notch receptor. *Journal of Cell Biology*, *166*(1), 73–83. https://doi.org/10.1083/jcb.200310098

Hansson, E. M., Strömberg, K., Bergśtedt, S., Yu, G., Näslund, J., Lundkvist, J., & Lendahl, U. (2005). Aph-1 interacts at the cell surface with proteins in the active γ-secretase complex and membrane-tethered Notch. *Journal of Neurochemistry*, *92*(5), 1010–1020. https://doi.org/10.1111/J.1471-4159.2004.02926.X

Henrique, D., & Schweisguth, F. (2019). Mechanisms of notch signaling: A simple logic deployed in time and space. *Development (Cambridge)*, *146*(3). https://doi.org/10.1242/dev.172148

Hori, K., Sen, A., & Artavanis-Tsakonas, S. (2013). Notch signaling at a glance. *Journal of Cell Science*, *126*(10), 2135–2140. https://doi.org/10.1242/jcs.127308

Housden, B. E., Fu, A. Q., Krejci, A., Bernard, F., Fischer, B., Tavaré, S., Russell, S., & Bray, S. J. (2013). Transcriptional Dynamics Elicited by a Short Pulse of Notch Activation Involves Feed-Forward Regulation by E(spl)/Hes Genes. *PLOS Genetics*, *9*(1), e1003162. https://doi.org/10.1371/JOURNAL.PGEN.1003162

Hung, V., Udeshi, N. D., Lam, S. S., Loh, K. H., Cox, K. J., Pedram, K., Carr, S. A., & Ting, A. Y. (2016). Spatially resolved proteomic mapping in living cells with the engineered peroxidase APEX2. *Nature Protocols*, *11*(3), 456–475. https://doi.org/10.1038/nprot.2016.018

Huttlin, E. L., Jedrychowski, M. P., Elias, J. E., Goswami, T., Rad, R., Beausoleil, S. A., Villén, J., Haas, W., Sowa, M. E., & Gygi, S. P. (2010). A tissue-specific atlas of mouse protein phosphorylation and expression. *Cell*, *143*(7), 1174–1189. https://doi.org/10.1016/j.cell.2010.12.001

Ilagan, M. X. G., Lim, S., Fulbright, M., Piwnica-Worms, D., & Kopan, R. (2011). Real-time imaging of Notch activation with a luciferase complementation-based reporter. *Science*

Signaling, *4*(181). https://doi.org/10.1126/SCISIGNAL.2001656/SUPPL_FILE/4_RS7_SM.PDF

Kalocsay, M. (2019). APEX Peroxidase-Catalyzed Proximity Labeling and Multiplexed Quantitative Proteomics. *Methods in Molecular Biology (Clifton, N.J.)*, *2008*, 41–55. https://doi.org/10.1007/978-1-4939-9537-0_4

Kamath, B. M., Bauer, R. C., Loomes, K. M., Chao, G., Gerfen, J., Hutchinson, A., Hardikar, W., Hirschfield, G., Jara, P., Krantz, I. D., Lapunzina, P., Leonard, L., Ling, S., Ng, V. L., le Hoang, P., Piccoli, D. A., & Spinner, N. B. (2012). NOTCH2 mutations in Alagille syndrome. *Journal of Medical Genetics*, *49*(2), 138–144. https://doi.org/10.1136/jmedgenet-2011-100544

Kirchhausen, T., Macia, E., & Pelish, H. E. (2008). Use of Dynasore, the Small Molecule Inhibitor of Dynamin, in the Regulation of Endocytosis. In *Methods in Enzymology* (Vol. 438, pp. 77–93). Methods Enzymol. https://doi.org/10.1016/S0076-6879(07)38006-3

Kobia, F., Duchi, S., Deflorian, G., & Vaccari, T. (2014). Pharmacologic inhibition of vacuolar H+ ATPase reduces physiologic and oncogenic Notch signaling. *Molecular Oncology*, *8*(2), 207–220. https://doi.org/10.1016/j.molonc.2013.11.002

Lam, S. S., Martell, J. D., Kamer, K. J., Deerinck, T. J., Ellisman, M. H., Mootha, V. K., & Ting, A. Y. (2015). Directed evolution of APEX2 for electron microscopy and proximity labeling. *Nature Methods*, *12*(1). https://doi.org/10.1038/nmeth.3179

Li, L., Krantz, I. D., Deng, Y., Genin, A., Banta, A. B., Collins, C. C., Qi, M., Trask, B. J., Kuo, W. L., Cochran, J., Costa, T., Pierpont, M. E. M., Rand, E. B., Piccoli, D. A., Hood, L., & Spinner, N. B. (1997). Alagille syndrome is caused by mutations in human Jagged1, which encodes a ligand for notch1. *Nature Genetics*, *16*(3), 243–251. https://doi.org/10.1038/ng0797-243

Louvet-Vallée, S. (2000). ERM proteins: From cellular architecture to cell signaling. In *Biology of the Cell* (Vol. 92, Issue 5, pp. 305–316). Elsevier Masson SAS. https://doi.org/10.1016/S0248-4900(00)01078-9

Ludwig, A., Hundhausen, C., Lambert, M., Broadway, N., Andrews, R., Bickett, D., Leesnitzer, M., & Becherer, J. (2005). Metalloproteinase inhibitors for the disintegrin-like metalloproteinases ADAM10 and ADAM17 that differentially block constitutive and phorbol ester-inducible shedding of cell surface molecules. *Combinatorial Chemistry & High Throughput Screening*, *8*(2), 161–171. https://doi.org/10.2174/1386207053258488

Macia, E., Ehrlich, M., Massol, R., Boucrot, E., Brunner, C., & Kirchhausen, T. (2006). Dynasore, a Cell-Permeable Inhibitor of Dynamin. *Developmental Cell*, *10*(6), 839–850. https://doi.org/10.1016/j.devcel.2006.04.002

Martin, A. P., Jacquemyn, M., Lipecka, J., Chhuon, C., Aushev, V. N., Meunier, B., Singh, M. K., Carpi, N., Piel, M., Codogno, P., Hergovich, A., Parrini, M. C., Zalcman, G., Guerrera, I. C., Daelemans, D., & Camonis, J. H. (2019). STK38 kinase acts as XPO1 gatekeeper regulating the nuclear export of autophagy proteins and other cargoes. *EMBO Reports*, *20*(11). https://doi.org/10.15252/embr.201948150

Mauthe, M., Orhon, I., Rocchi, C., Zhou, X., Luhr, M., Hijlkema, K. J., Coppes, R. P., Engedal, N., Mari, M., & Reggiori, F. (2018). Chloroquine inhibits autophagic flux by decreasing

autophagosome-lysosome fusion. *Autophagy*, *14*(8), 1435–1455. https://doi.org/10.1080/15548627.2018.1474314

May, E. A., Kalocsay, M., D'Auriac, I. G., Schuster, P. S., Gygi, S. P., Nachury, M. v., & Mick, D. U. (2021). Time-resolved proteomics profiling of the ciliary Hedgehog response. *The Journal of Cell Biology*, *220*(5). https://doi.org/10.1083/jcb.202007207

McAlister, G. C., Nusinow, D. P., Jedrychowski, M. P., Wühr, M., Huttlin, E. L., Erickson, B. K., Rad, R., Haas, W., & Gygi, S. P. (2014). MultiNotch MS3 enables accurate, sensitive, and multiplexed detection of differential expression across cancer cell line proteomes. *Analytical Chemistry*, *86*(14), 7150–7158. https://doi.org/10.1021/ac502040v

Mccluskey, A., Daniel, J. A., Hadzic, G., Chau, N., Clayton, E. L., Mariana, A., Whiting, A., Gorgani, N. N., Lloyd, J., Quan, A., Moshkanbaryans, L., Krishnan, S., Perera, S., Chircop, M., von Kleist, L., Mcgeachie, A. B., Howes, M. T., Parton, R. G., Campbell, M., … Robinson, P. J. (2013). Building a better dynasore: The dyngo compounds potently inhibit dynamin and endocytosis. *Traffic*, *14*(12), 1272–1289. https://doi.org/10.1111/tra.12119

Mittal, P., & Roberts, C. W. M. (2020). The SWI/SNF complex in cancer — biology, biomarkers and therapy. In *Nature Reviews Clinical Oncology* (Vol. 17, Issue 7, pp. 435–448). Nature Research. https://doi.org/10.1038/s41571-020-0357-3

Nam, Y., Sliz, P., Song, L., Aster, J. C., & Blacklow, S. C. (2006). Structural basis for cooperativity in recruitment of MAML coactivators to Notch transcription complexes. *Cell*, *124*(5), 973–983. https://doi.org/10.1016/j.cell.2005.12.037

Oswald, F., Täuber, B., Dobner, T., Bourteele, S., Kostezka, U., Adler, G., Liptay, S., & Schmid, R. M. (2001). p300 acts as a transcriptional coactivator for mammalian Notch-1. *Molecular and Cellular Biology*, *21*(22), 7761–7774. https://doi.org/10.1128/MCB.21.22.7761-7774.2001

Paek, J., Kalocsay, M., Staus, D. P., Wingler, L., Pascolutti, R., Paulo, J. A., Gygi, S. P., & Kruse, A. C. (2017). Multidimensional Tracking of GPCR Signaling via Peroxidase-Catalyzed Proximity Labeling. *Cell*, *169*(2), 338-349.e11. https://doi.org/10.1016/j.cell.2017.03.028

Park, H., Hundley, F. v., Yu, Q., Overmyer, K. A., Brademan, D. R., Serrano, L., Paulo, J. A., Paoli, J. C., Swarup, S., Coon, J. J., Gygi, S. P., & Wade Harper, J. (2022). Spatial snapshots of amyloid precursor protein intramembrane processing via early endosome proteomics. *Nature Communications 2022 13:1*, *13*(1), 1–21. https://doi.org/10.1038/s41467-022-33881-x

Paulo, J. A., O'Connell, J. D., Everley, R. A., O'Brien, J., Gygi, M. A., & Gygi, S. P. (2016). Quantitative mass spectrometry-based multiplexing compares the abundance of 5000 S. cerevisiae proteins across 10 carbon sources. *Journal of Proteomics*, *148*, 85–93. https://doi.org/10.1016/j.jprot.2016.07.005

Petcherski, A. G., & Kimble, J. (2000). Mastermind is a putative activator for Notch [1]. In *Current Biology* (Vol. 10, Issue 13). Current Biology Ltd. https://doi.org/10.1016/S0960-9822(00)00577-7

Pillidge, Z., & Bray, S. J. (2019). SWI / SNF chromatin remodeling controls Notch-responsive enhancer accessibility . *EMBO Reports*, *20*(5). https://doi.org/10.15252/embr.201846944

Ran, F. A., Hsu, P. D., Wright, J., Agarwala, V., Scott, D. A., & Zhang, F. (2013). Genome engineering using the CRISPR-Cas9 system. *Nature Protocols*, *8*(11), 2281–2308. https://doi.org/10.1038/nprot.2013.143

Rappsilber, J., Mann, M., & Ishihama, Y. (2007). Protocol for micro-purification, enrichment, pre-fractionation and storage of peptides for proteomics using StageTips. *Nature Protocols*, *2*(8), 1896–1906. https://doi.org/10.1038/nprot.2007.261

Rhee, H.-W., Zou, P., Udeshi, N. D., Martell, J. D., Mootha, V. K., Carr, S. a, & Ting, A. Y. (2013). Proteomic Mapping of Mitochondria in Living Cells via Spatially Restricted Enzymatic Tagging. *Science*, *1328*(2013). https://doi.org/10.1126/science.1230593

Rogers, J. M., Guo, B., Egan, E. D., Aster, J. C., Adelman, K., & Blacklow, S. C. (2020). MAML1-Dependent Notch-Responsive Genes Exhibit Differing Cofactor Requirements for Transcriptional Activation. *Molecular and Cellular Biology*, *40*(11). https://doi.org/10.1128/mcb.00014-20

Schindelin, J., Arganda-Carreras, I., Frise, E., Kaynig, V., Longair, M., Pietzsch, T., Preibisch, S., Rueden, C., Saalfeld, S., Schmid, B., Tinevez, J. Y., White, D. J., Hartenstein, V., Eliceiri, K., Tomancak, P., & Cardona, A. (2012). Fiji: An open-source platform for biological-image analysis. In *Nature Methods* (Vol. 9, Issue 7, pp. 676–682). Nature Publishing Group. https://doi.org/10.1038/nmeth.2019

Seaman, M. N. J. (2012). The retromer complex-endosomal protein recycling and beyond. In *Journal of Cell Science* (Vol. 125, Issue 20, pp. 4693–4702). Company of Biologists. https://doi.org/10.1242/jcs.103440

Shanmugam, V., Craig, J. W., Hilton, L. K., Nguyen, M. H., Rushton, C. K., Fahimdanesh, K., Lovitch, S., Ferland, B., Scott, D. W., & Aster, J. C. (2021). Notch activation is pervasive in SMZL and uncommon in DLBCL: implications for Notch signaling in B-cell tumors. *Blood Advances*, *5*(1), 71. https://doi.org/10.1182/BLOODADVANCES.2020002995

Siebel, C., & Lendahl, U. (2017). Notch signaling in development, tissue homeostasis, and disease. *Physiological Reviews*, *97*(4), 1235–1294. https://doi.org/10.1152/physrev.00005.2017

Simpson, M. A., Irving, M. D., Asilmaz, E., Gray, M. J., Dafou, D., Elmslie, F. v., Mansour, S., Holder, S. E., Brain, C. E., Burton, B. K., Kim, K. H., Pauli, R. M., Aftimos, S., Stewart, H., Kim, C. A., Holder-Espinasse, M., Robertson, S. P., Drake, W. M., & Trembath, R. C. (2011). Mutations in NOTCH2 cause Hajdu-Cheney syndrome, a disorder of severe and progressive bone loss. *Nature Genetics 2011 43:4*, *43*(4), 303–305. https://doi.org/10.1038/ng.779

Sprinzak, D., & Blacklow, S. C. (2021). Biophysics of Notch Signaling. *Annual Review of Biophysics*, *50*(1), 157–189. https://doi.org/10.1146/annurev-biophys-101920-082204

Turnpenny, P. D., Whittock, N., Duncan, J., Dunwoodie, S., Kusumi, K., & Ellard, S. (2003). Novel mutations in DLL3, a somitogenesis gene encoding a ligand for the Notch signalling pathway, cause a consistent pattern of abnormal vertebral segmentation in spondylocostal dysostosis. *Journal of Medical Genetics*, *40*(5), 333. https://doi.org/10.1136/JMG.40.5.333

Vaccari, T., Duchi, S., Cortese, K., Tacchetti, C., & Bilder, D. (2010). The vacuolar ATPase is required for physiological as well as pathological activation of the Notch receptor. *Development*, *137*(11), 1825–1832. https://doi.org/10.1242/dev.045484

Varnum-Finney, B., Brashem-Stein, C., & Bernstein, I. D. (2003). Combined effects of Notch signaling and cytokines induce a multiple log increase in precursors with lymphoid and

myeloid reconstituting ability. *Blood*, *101*(5), 1784–1789. https://doi.org/10.1182/BLOOD-2002-06-1862

Wälde, S., Thakar, K., Hutten, S., Spillner, C., Nath, A., Rothbauer, U., Wiemann, S., & Kehlenbach, R. H. (2012). The Nucleoporin Nup358/RanBP2 Promotes Nuclear Import in a Cargo- and Transport Receptor-Specific Manner. *Traffic*, *13*(2), 218–233. https://doi.org/10.1111/j.1600-0854.2011.01302.x

Wallberg, A. E., Pedersen, K., Lendahl, U., & Roeder, R. G. (2002). p300 and PCAF act cooperatively to mediate transcriptional activation from chromatin templates by notch intracellular domains in vitro. *Molecular and Cellular Biology*, *22*(22), 7812–7819. https://doi.org/10.1128/MCB.22.22.7812-7819.2002

Wang, H., Zang, C., Taing, L., Arnett, K. L., Wong, Y. J., Pear, W. S., Blacklow, S. C., Liu, X. S., & Aster, J. C. (2014). NOTCH1-RBPJ complexes drive target gene expressionthrough dynamic interactions with superenhancers. *Proceedings of the National Academy of Sciences of the United States of America*, *111*(2), 705–710. https://doi.org/10.1073/PNAS.1315023111/SUPPL_FILE/PNAS.201315023SI.PDF

Wang, N. J., Sanborn, Z., Arnett, K. L., Bayston, L. J., Liao, W., Proby, C. M., Leigh, I. M., Collisson, E. A., Gordon, P. B., Jakkula, L., Pennypacker, S., Zou, Y., Sharma, M., North, J. P., Vemula, S. S., Mauro, T. M., Neuhaus, I. M., LeBoit, P. E., Hur, J. S., … Cho, R. J. (2011). Loss-of-function mutations in Notch receptors in cutaneous and lung squamous cell carcinoma. *Proceedings of the National Academy of Sciences of the United States of America*, *108*(43), 17761–17766. https://doi.org/10.1073/PNAS.1114669108

Wu, L., Aster, J. C., Blacklow, S. C., Lake, R., Artavanis-Tsakonas, S., & Griffin, J. D. (2000). MAML1, a human homologue of Drosophila mastermind, is a transcriptional co-activator for NOTCH receptors. *Nature Genetics*, *26*(4), 484–489. https://doi.org/10.1038/82644

Xu, J., Feng, H. T., Wang, C., Yip, K. H. M., Pavlos, N., Papadimitriou, J. M., Wood, D., & Zheng, M. H. (2003). Effects of bafilomycin A1: An inhibitor of vacuolar H (+)-ATPases on endocytosis and apoptosis in RAW cells and RAW cell-derived osteoclasts. *Journal of Cellular Biochemistry*, *88*(6), 1256–1264. https://doi.org/10.1002/jcb.10477

Yokoyama, N., Hayashi, N., Seki, T., Panté, N., Ohba, T., Nishii, K., Kuma, K., Hayashida, T., Miyata, T., Aebi, U., Fukui, M., & Nishimoto, T. (1995). A giant nucleopore protein that binds Ran/TC4. *Nature*, *376*(6536), 184–188. https://doi.org/10.1038/376184a0

Yoshimori, T., Yamamoto, A., Moriyama, Y., Futai, M., & Tashiro, Y. (1991). Bafilomycin A1, a specific inhibitor of vacuolar-type H+-ATPase, inhibits acidification and protein degradation in lysosomes of cultured cells. *Journal of Biological Chemistry*, *266*(26), 17707–17712. https://doi.org/10.1016/s0021-9258(19)47429-2

Figure 1

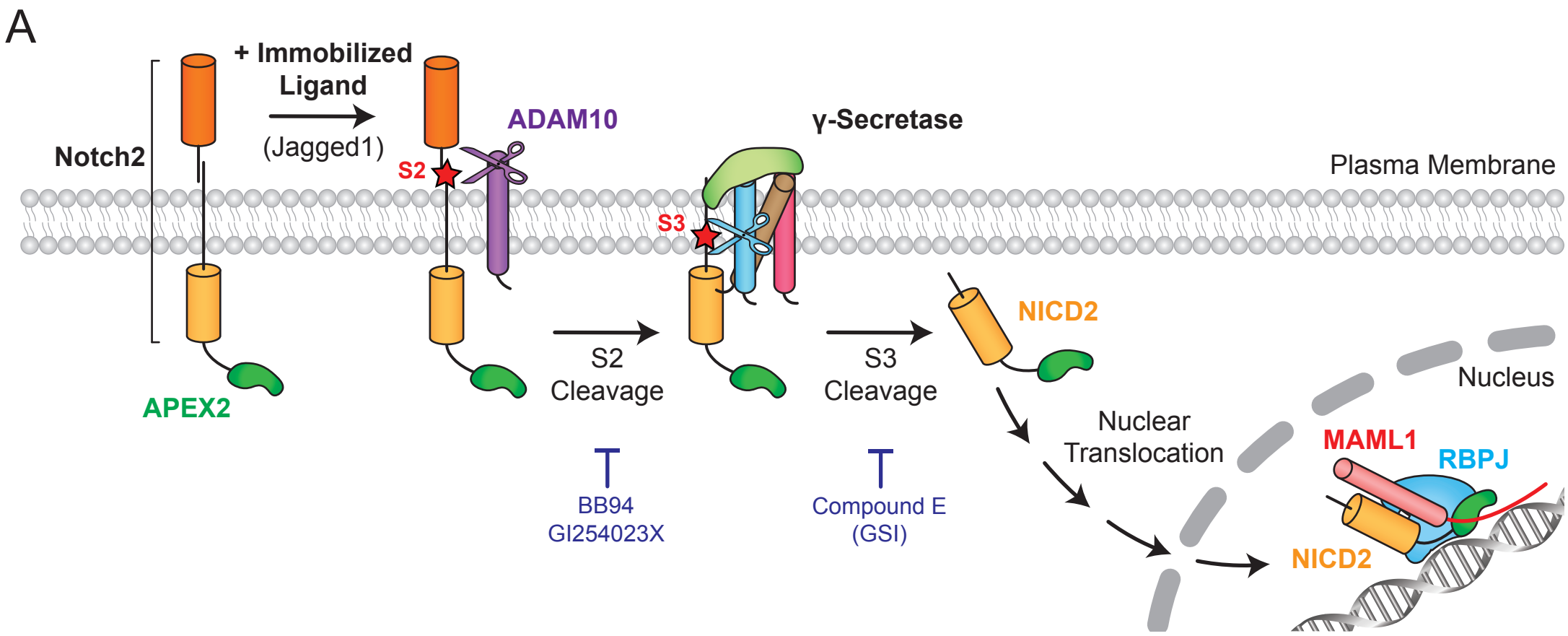

Figure 2

Figure 3

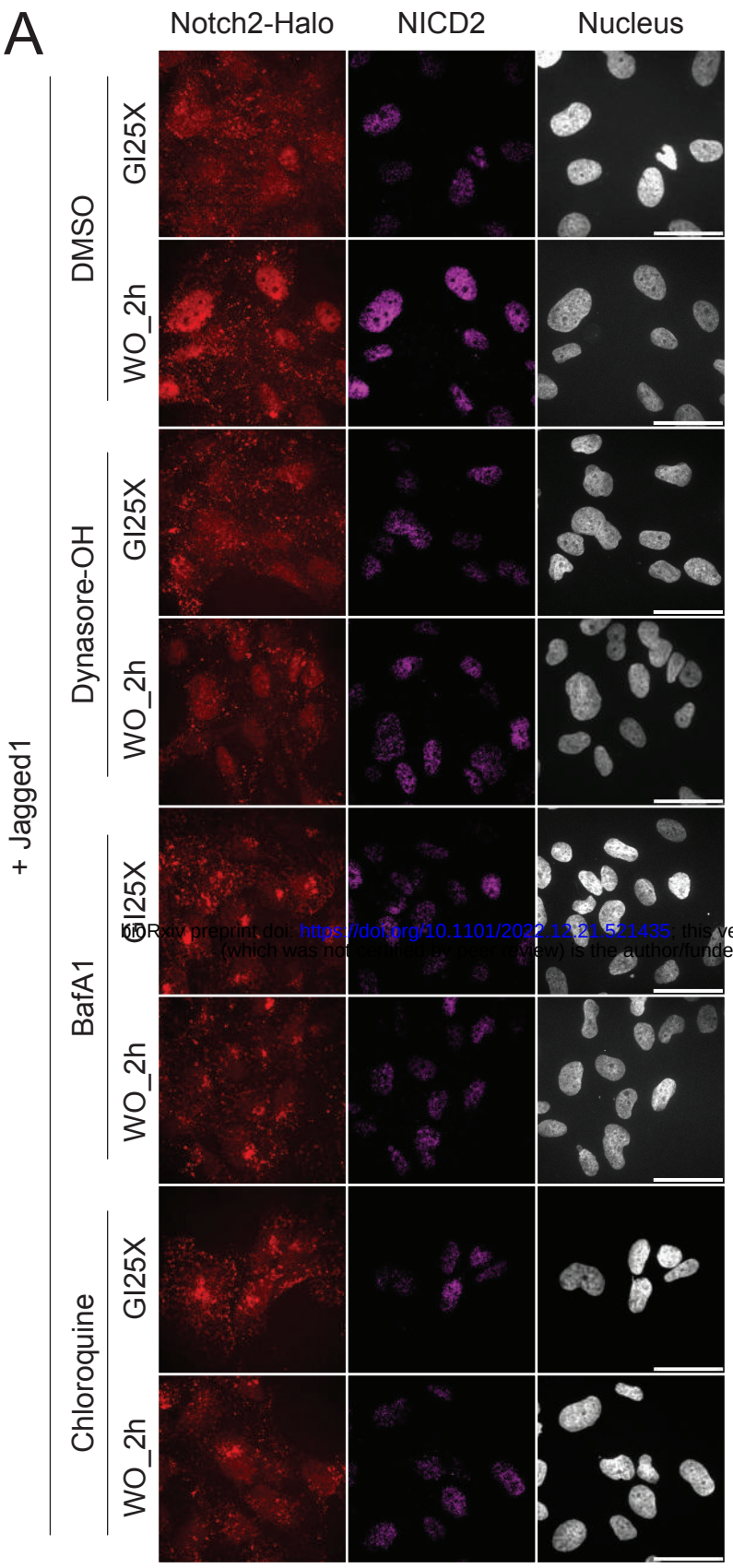

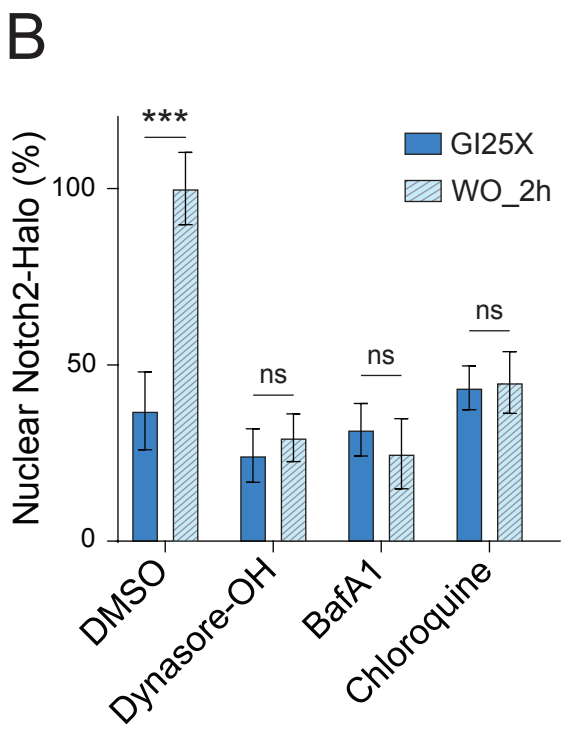

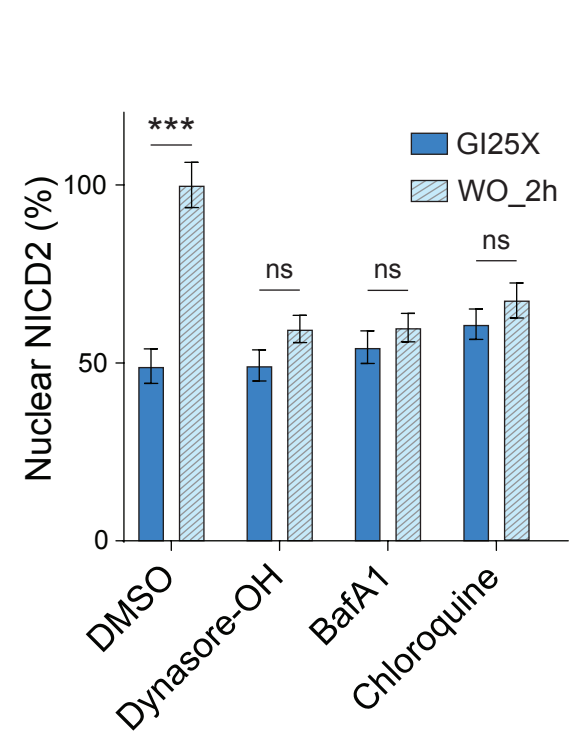

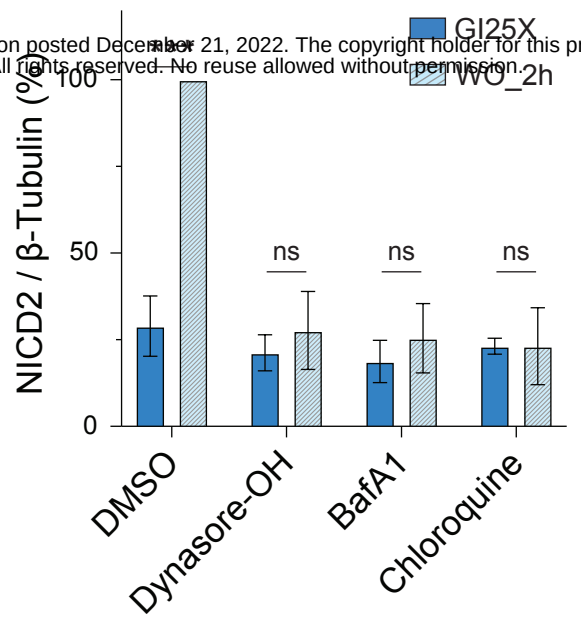

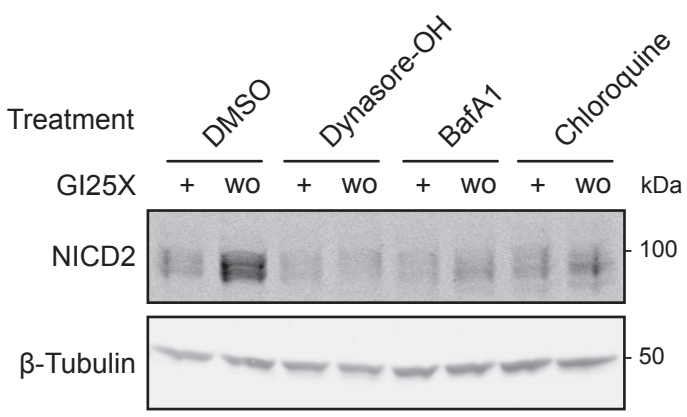

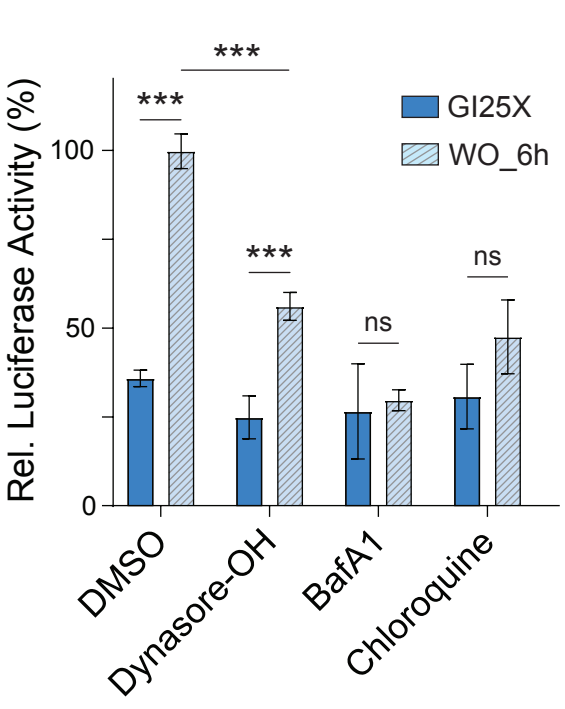

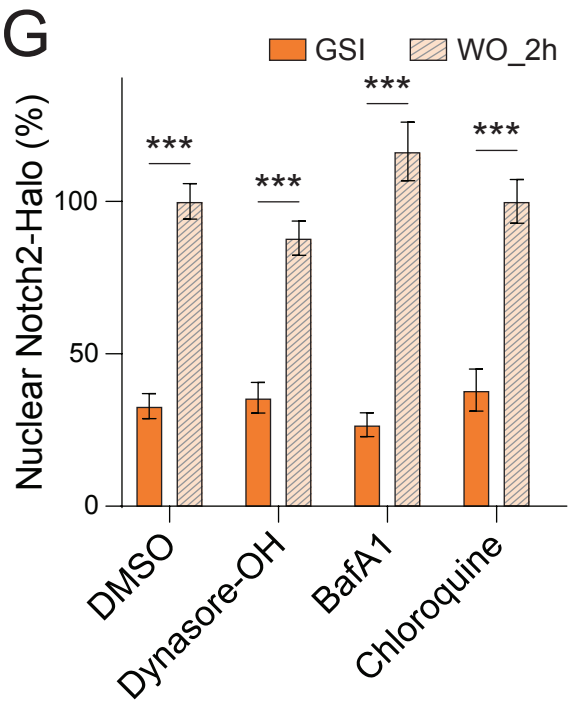

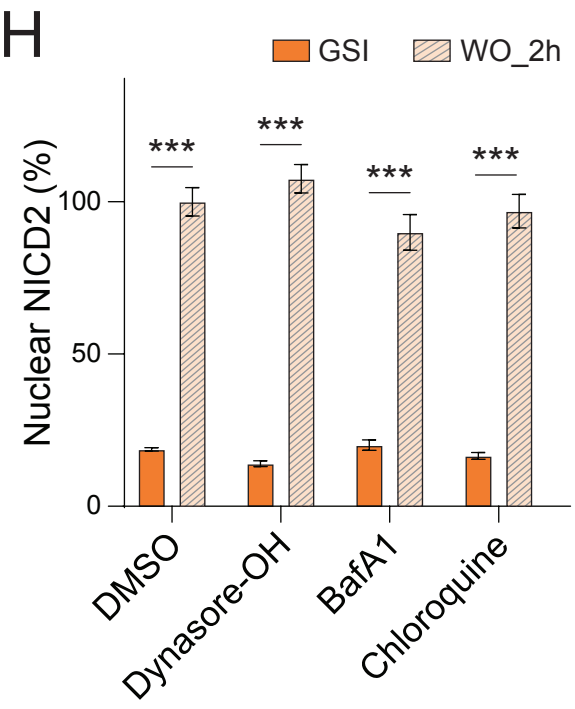

Figure 4

Figure 5

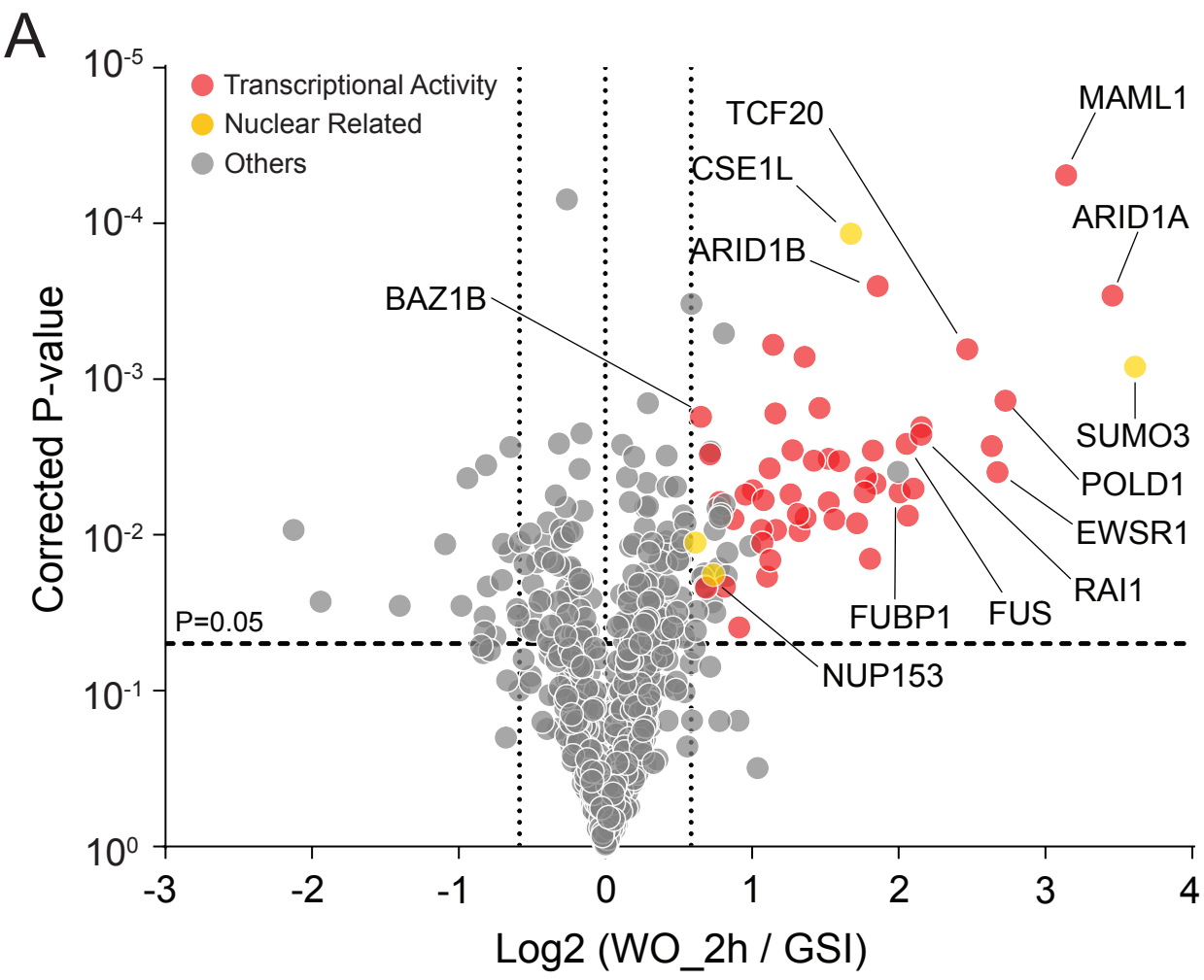

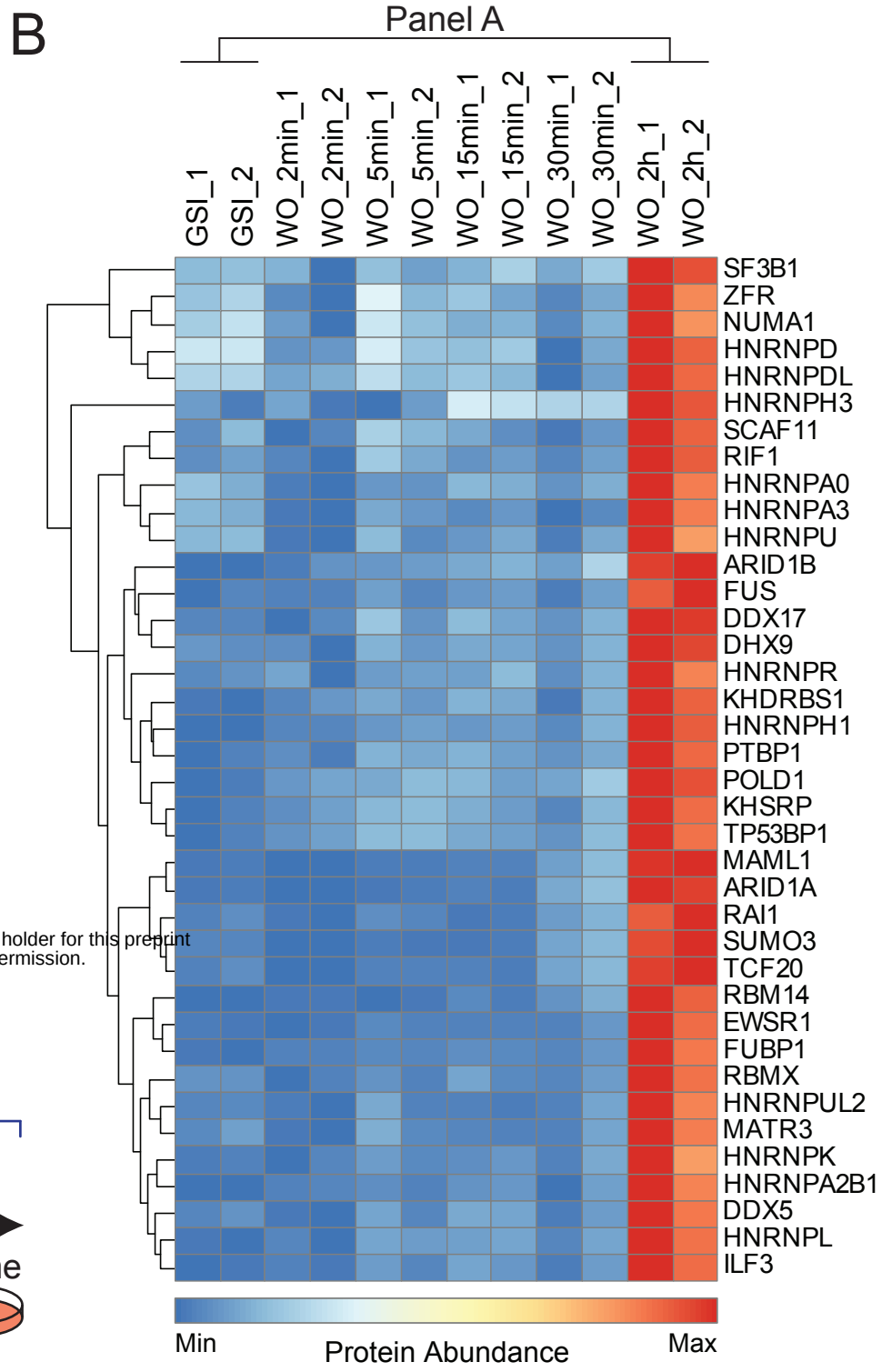

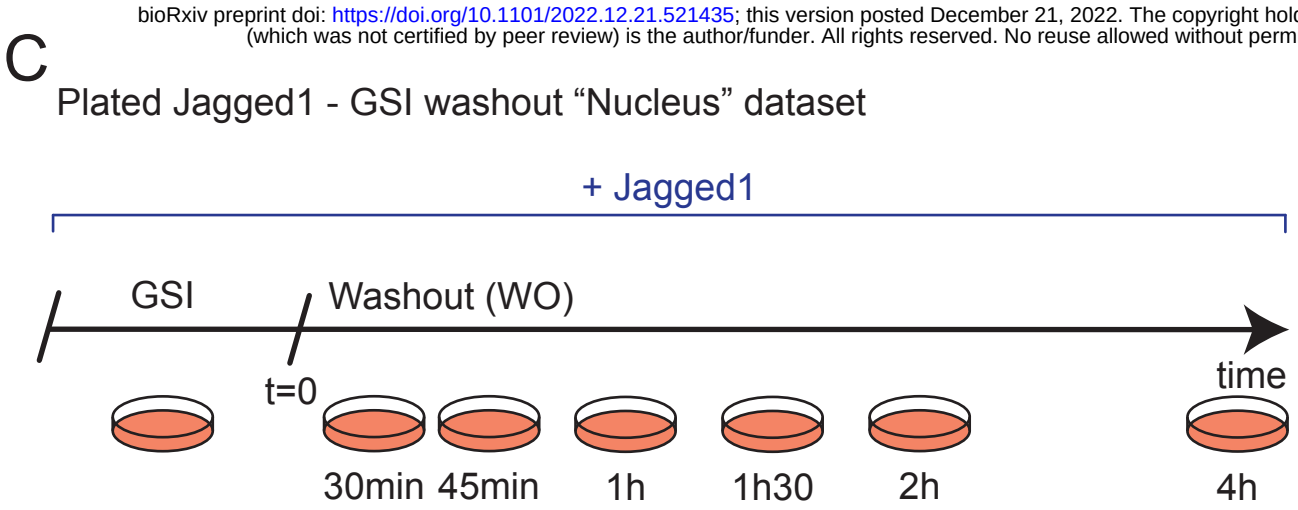

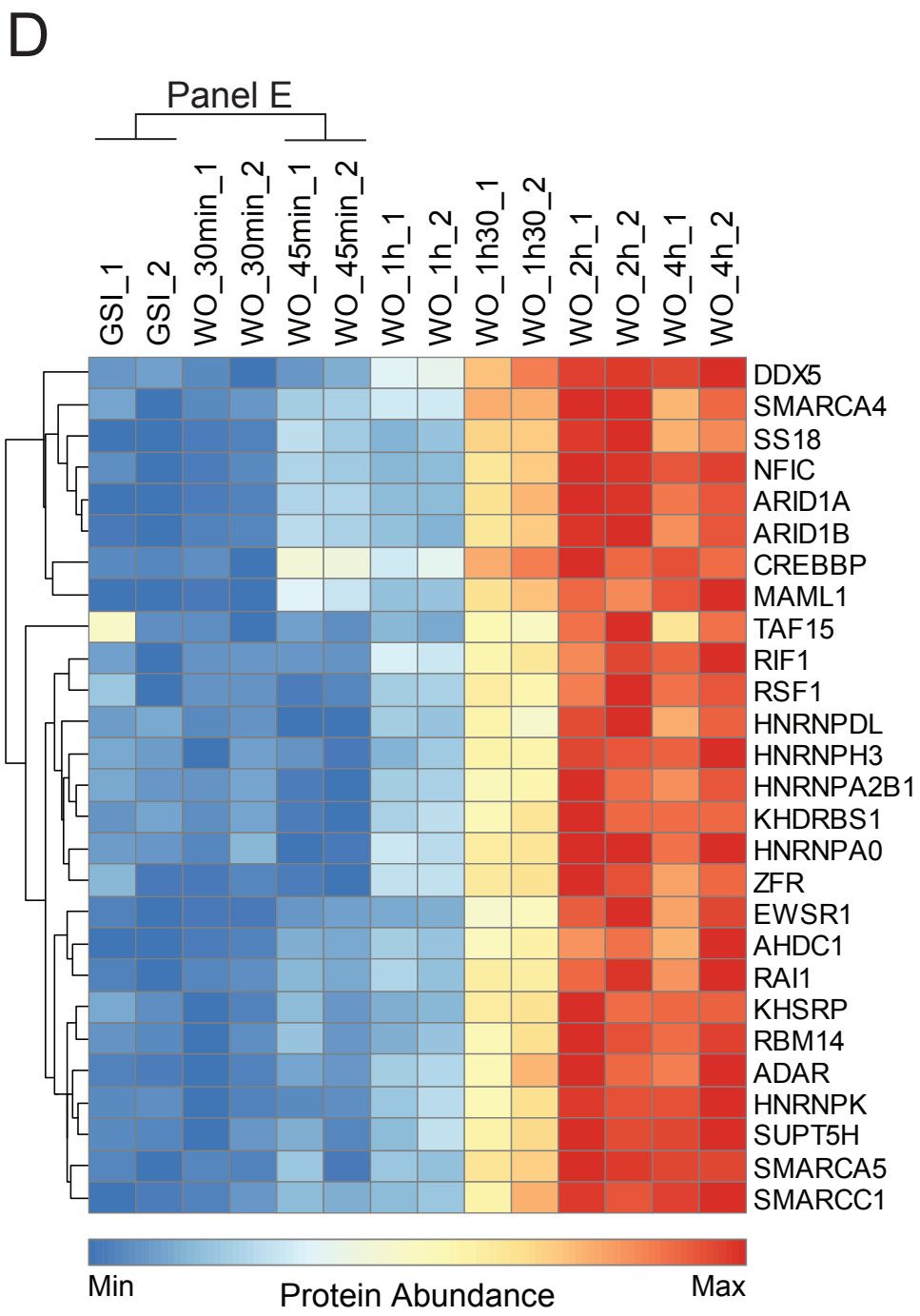

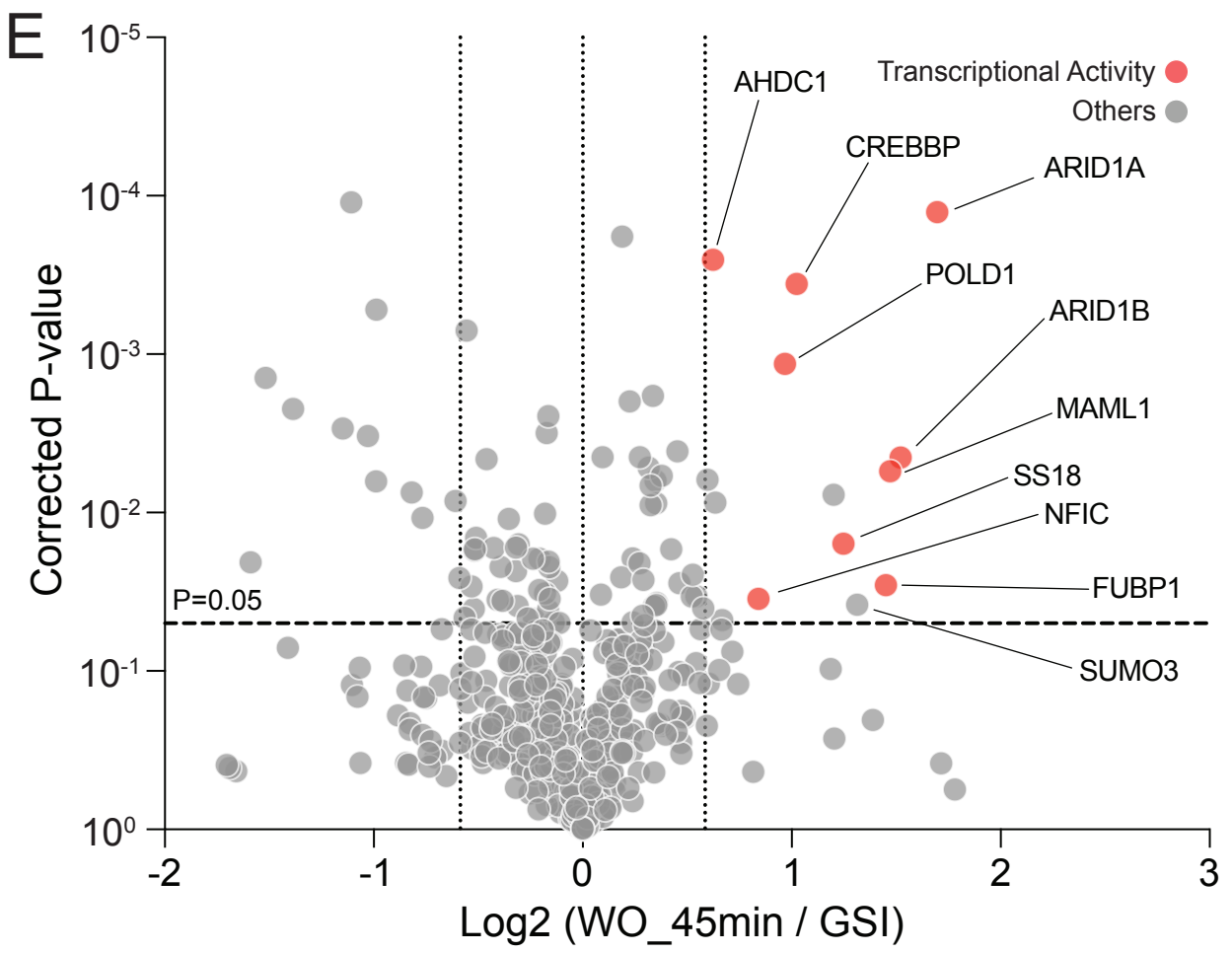

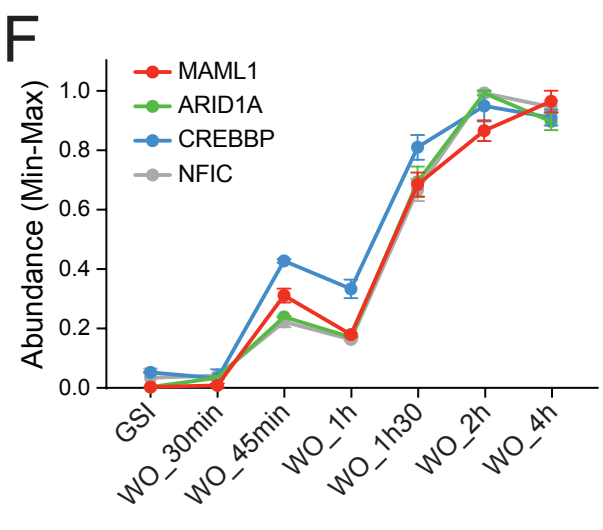

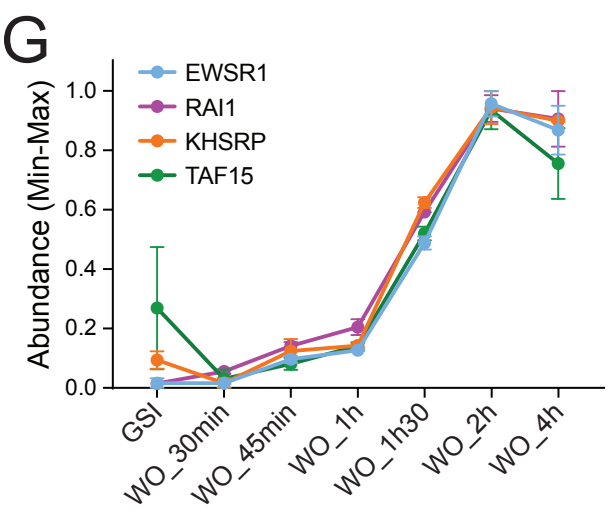

Figure 6

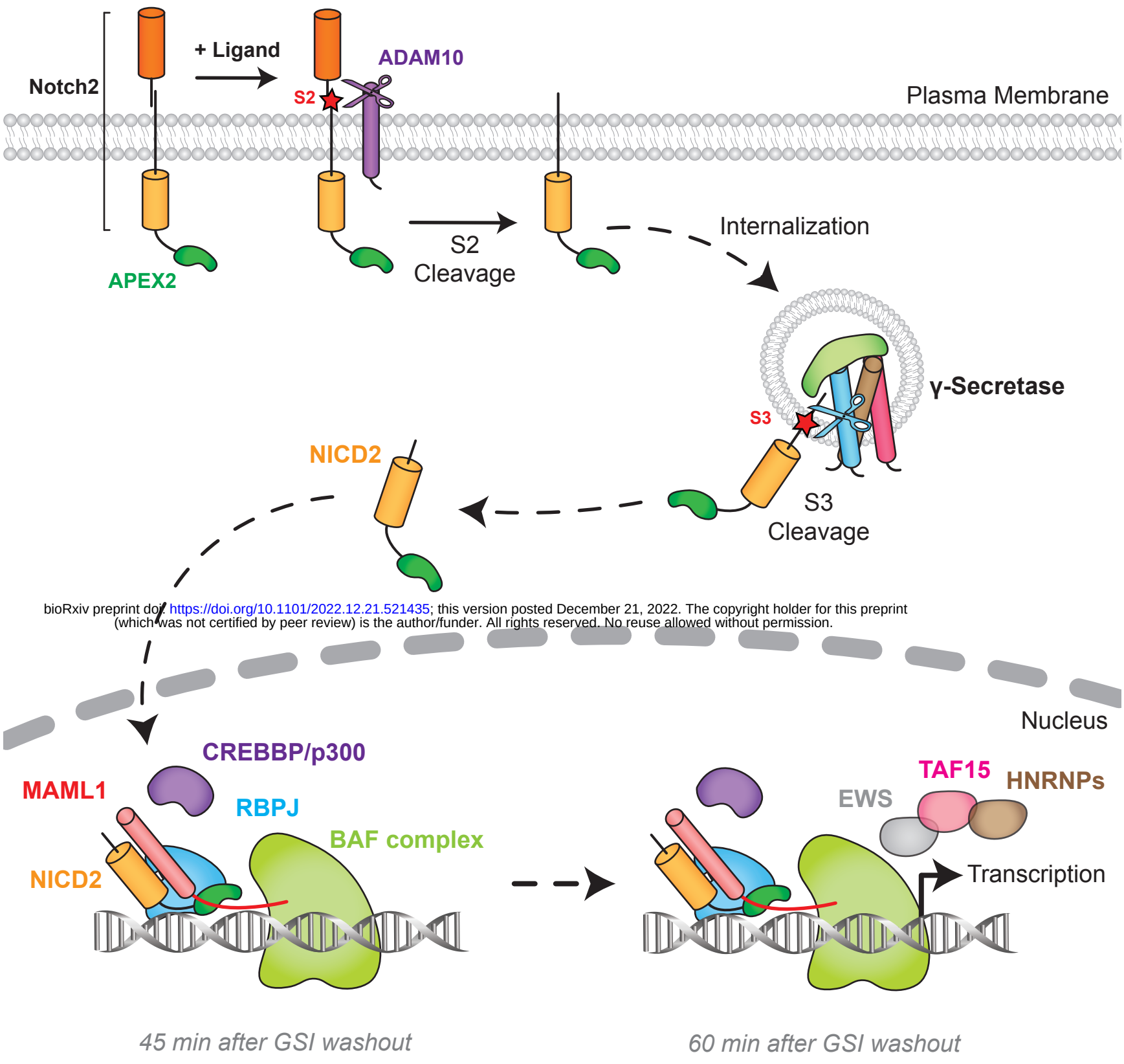

Supplemental Figure 1

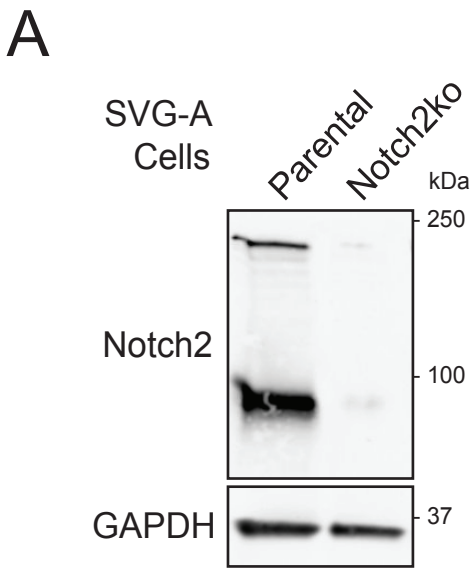

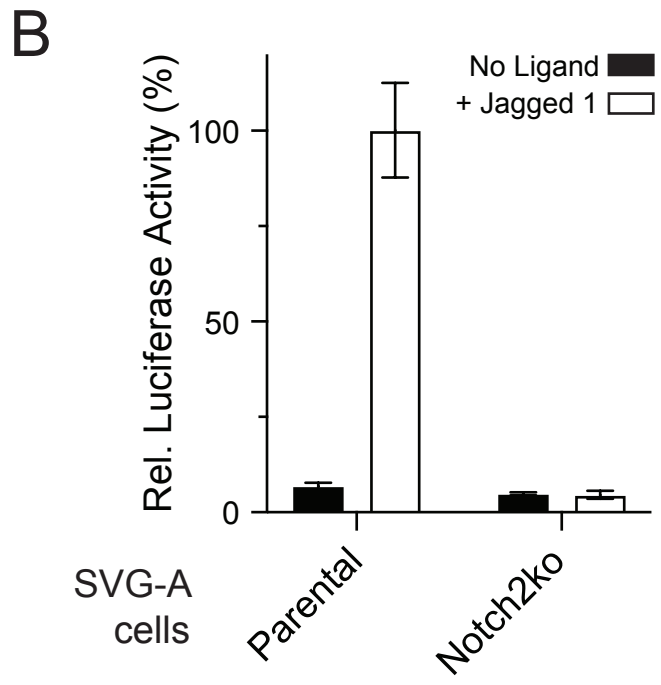

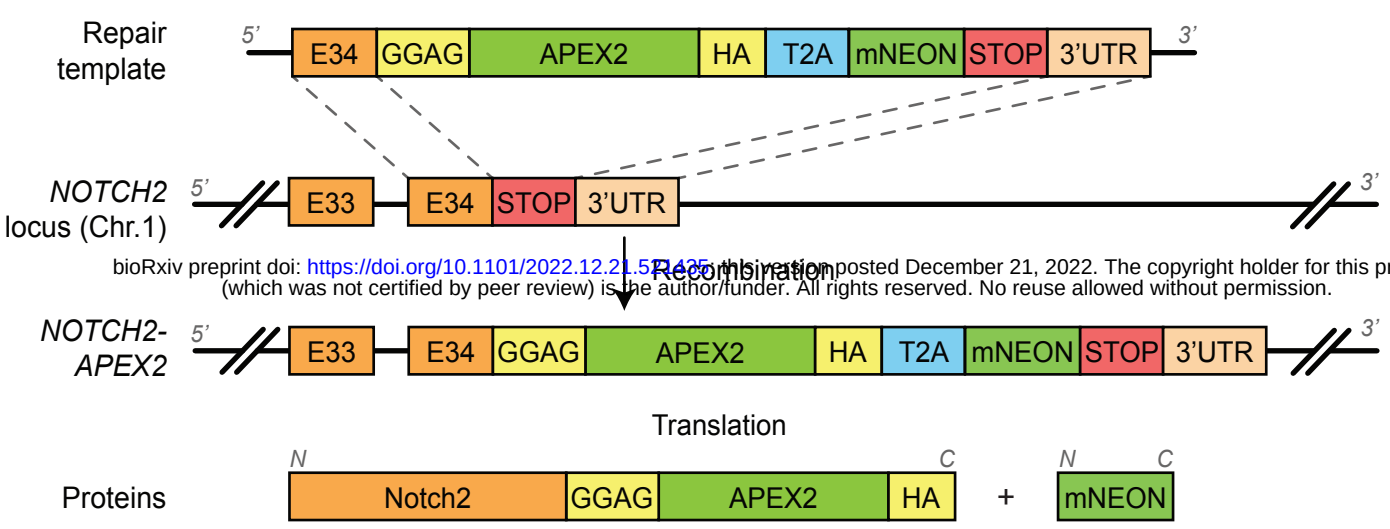

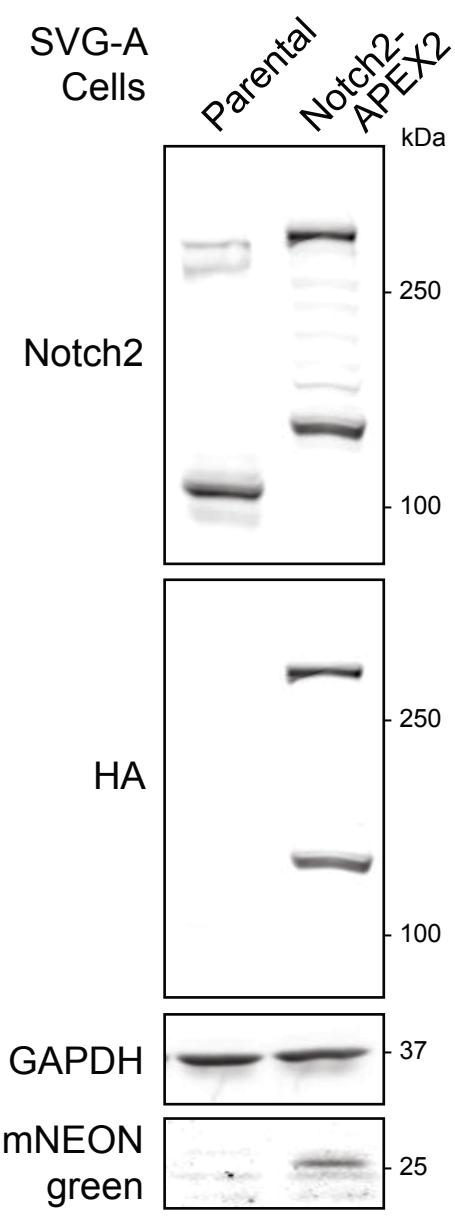

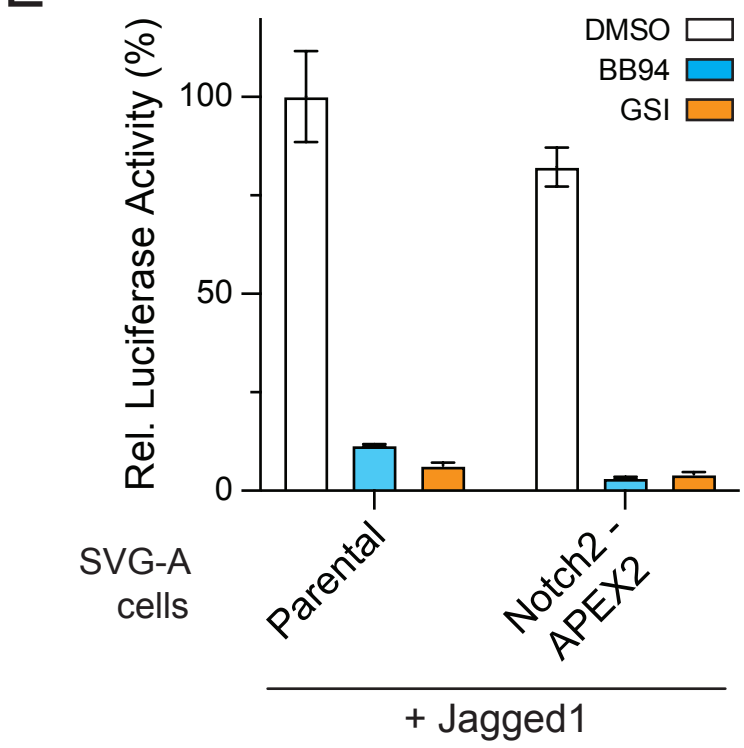

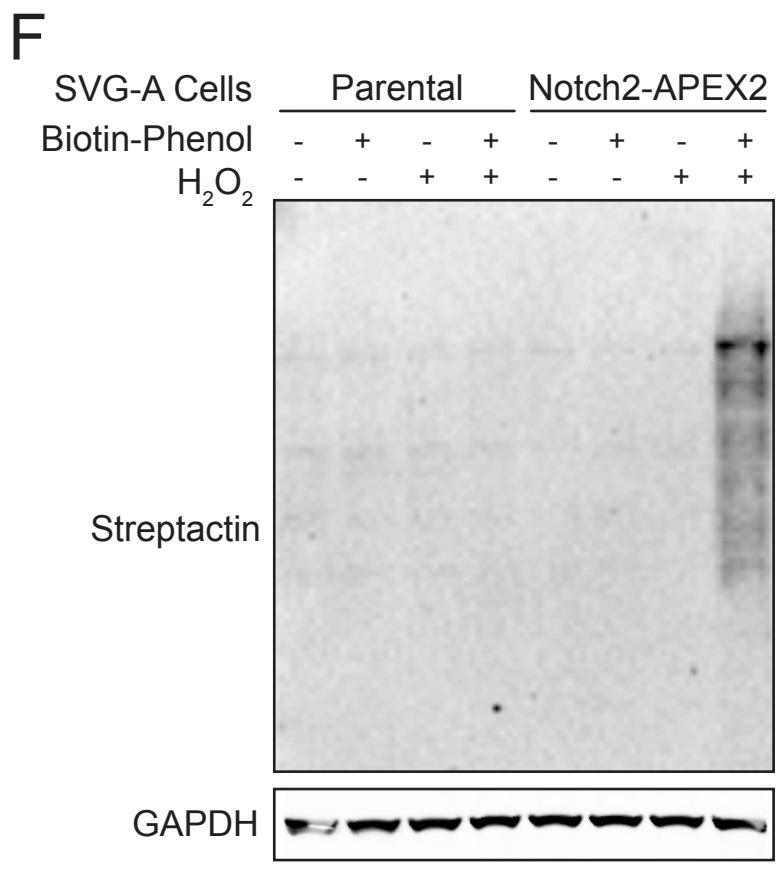

Supplemental Figure 2

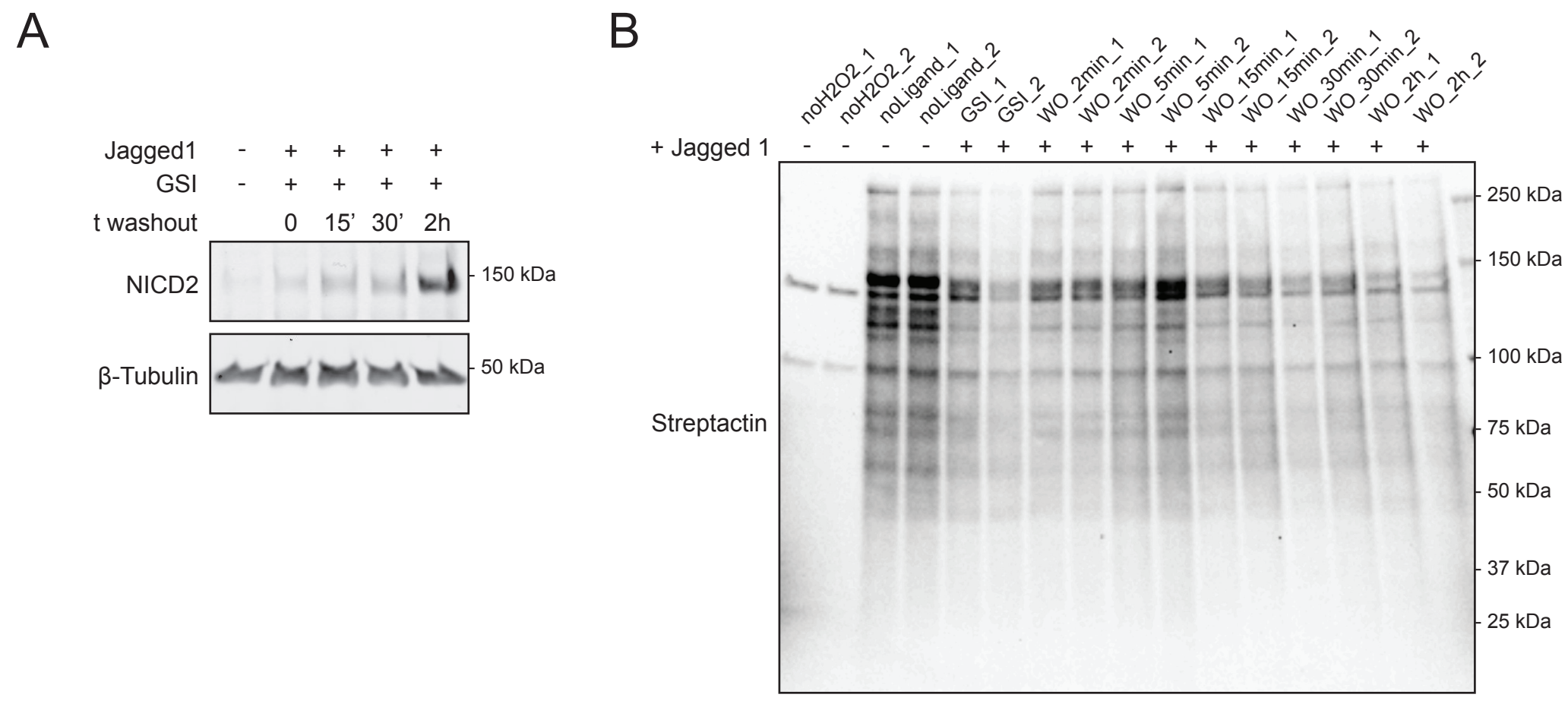

Supplemental Figure 3

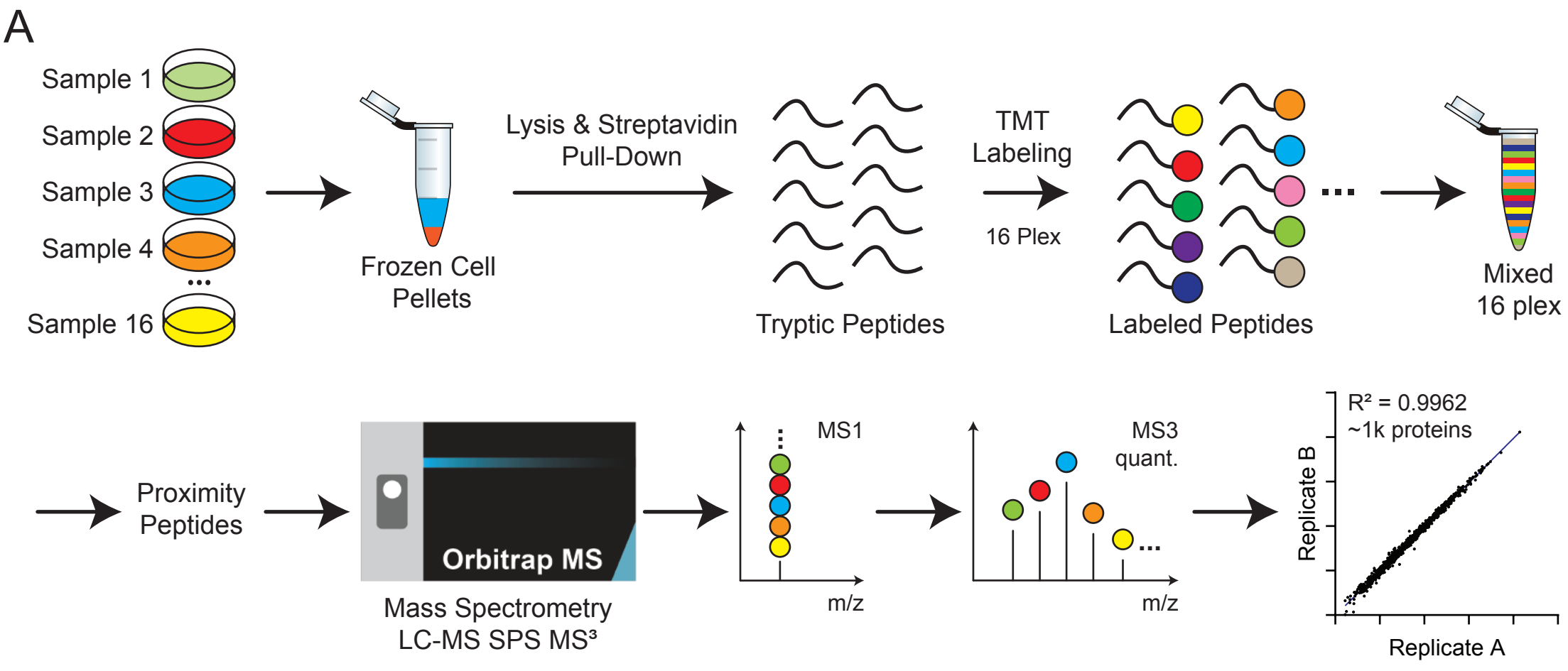

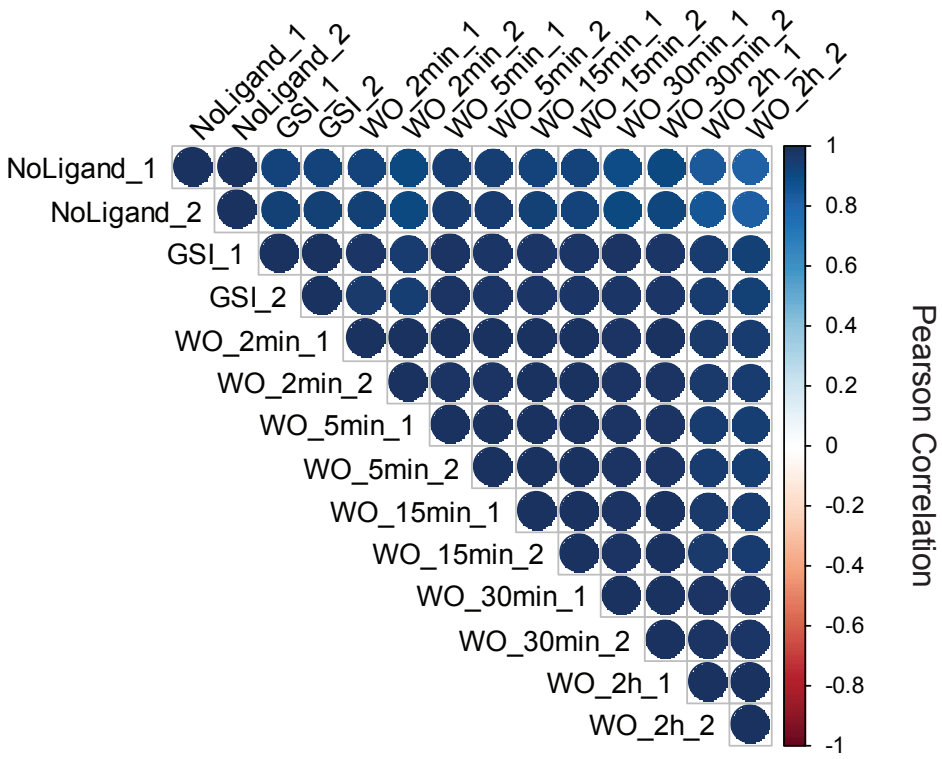

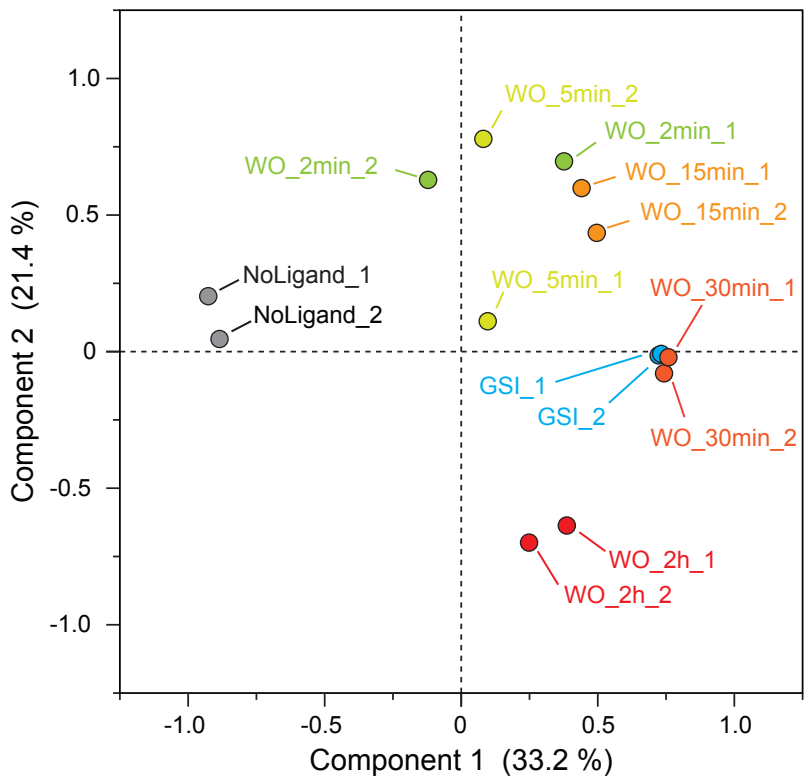

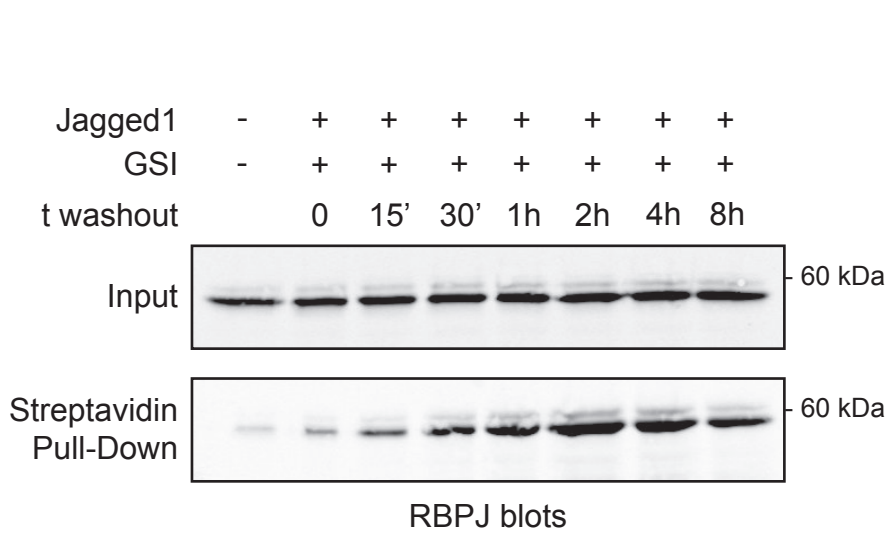

Supplemental Figure 4

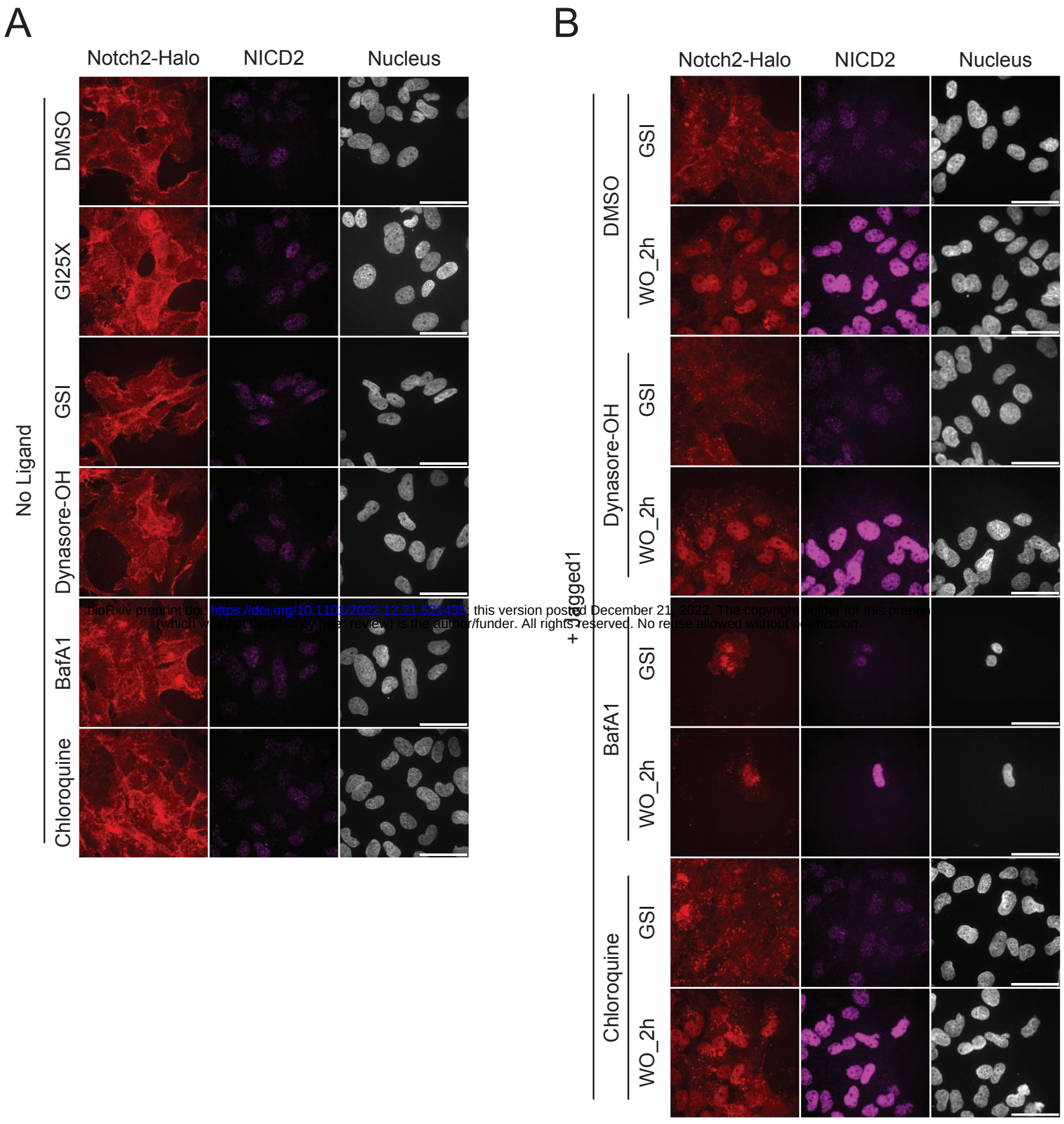

Supplemental Figure 5

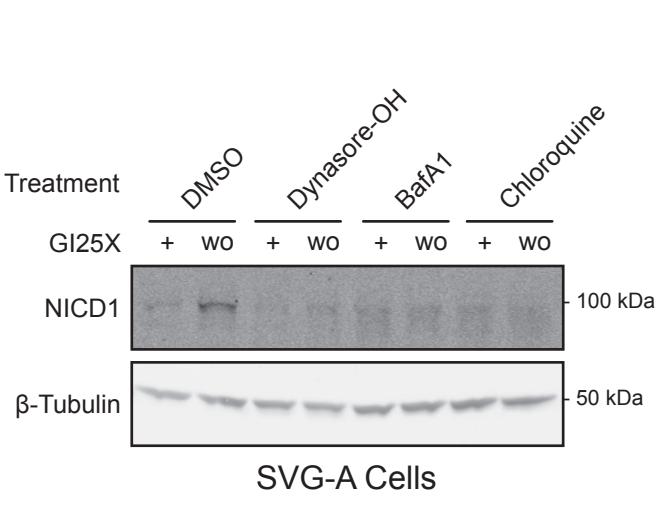

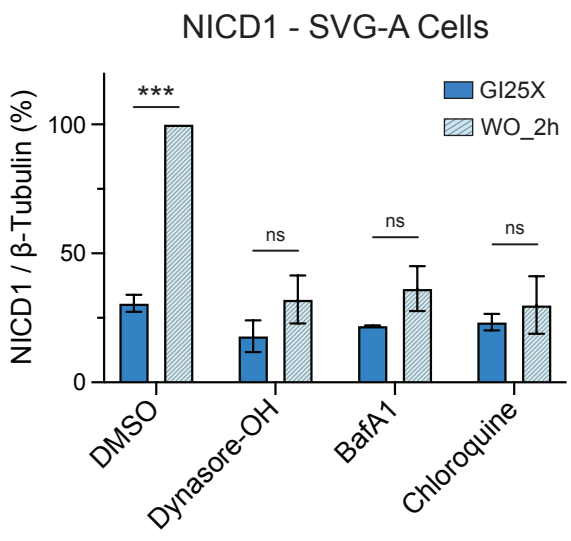

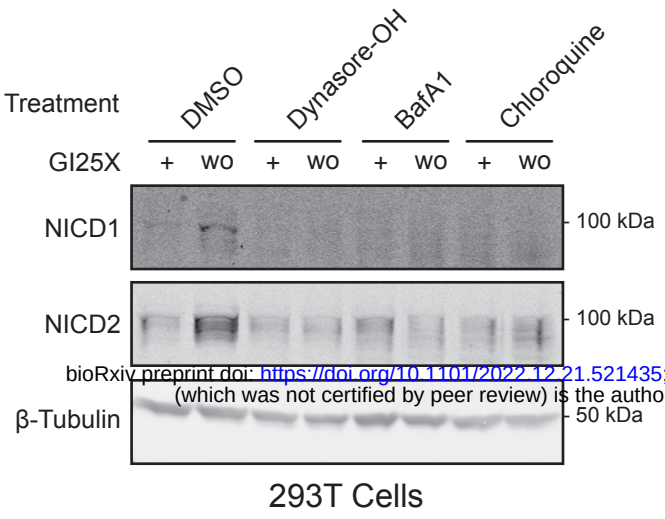

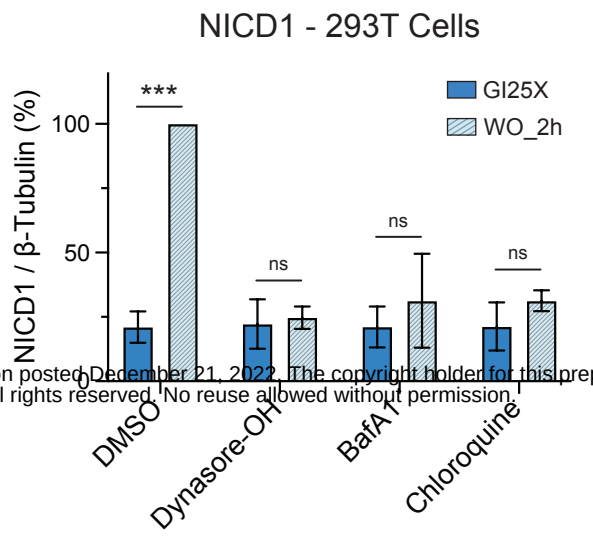

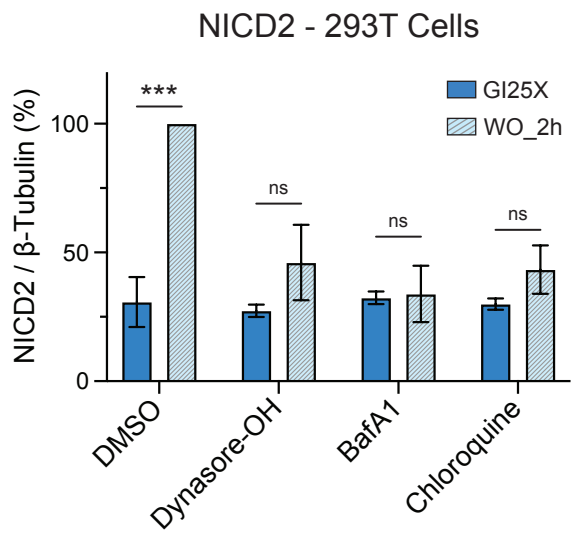

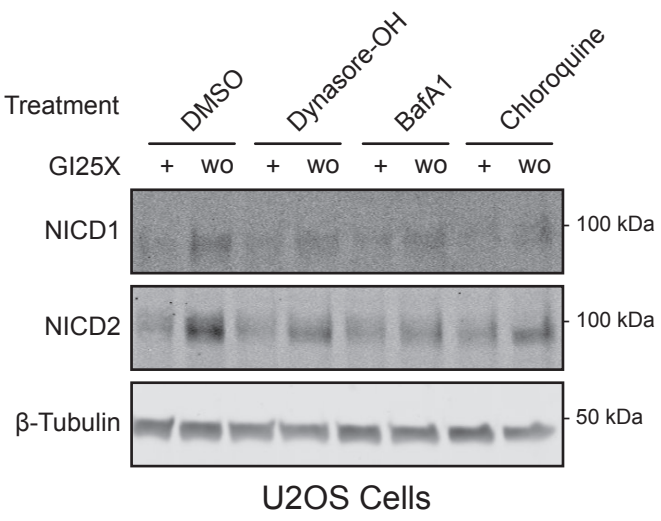

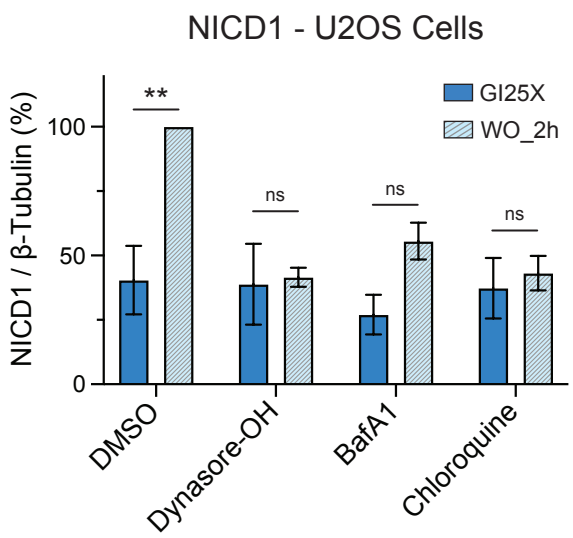

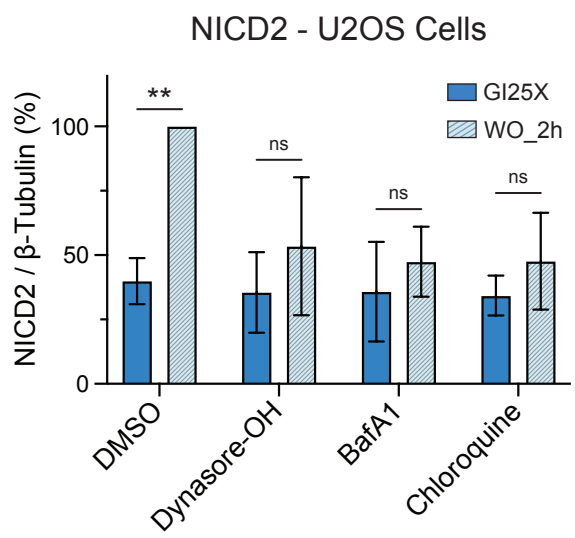

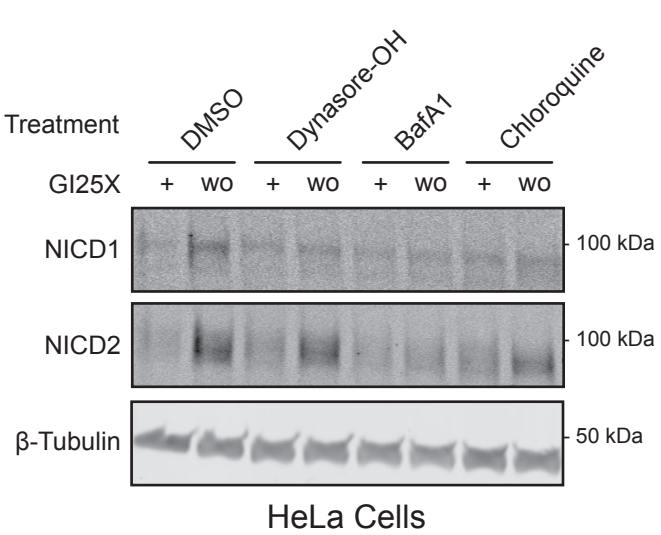

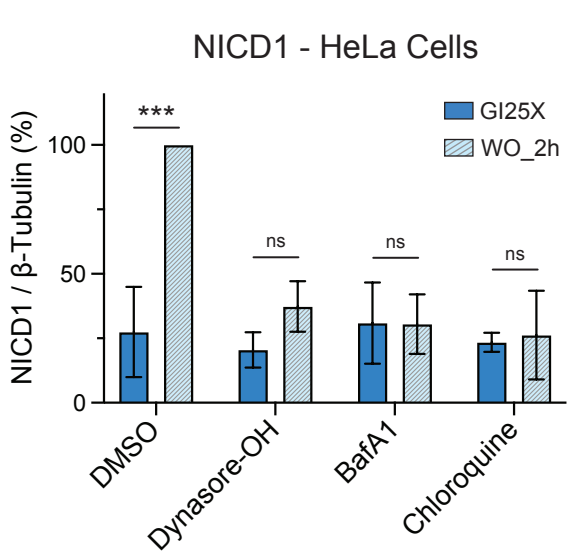

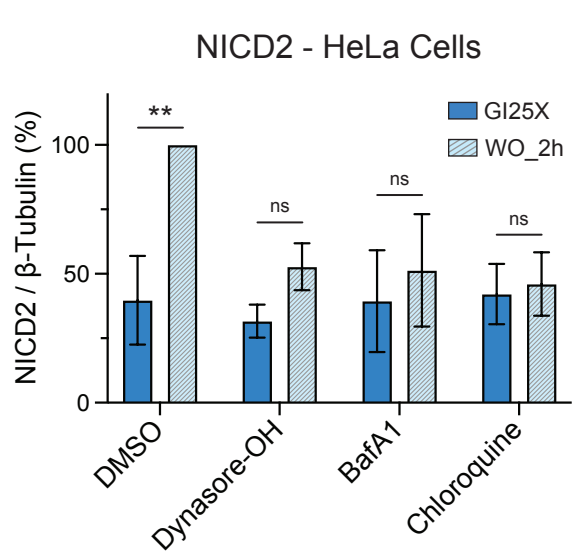

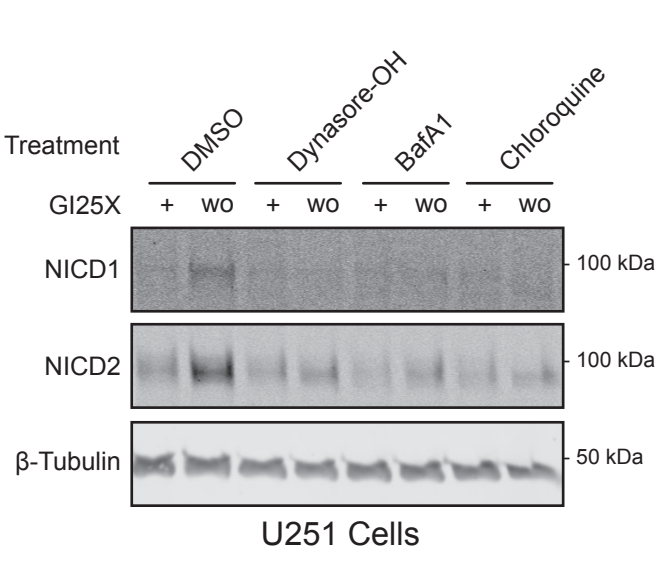

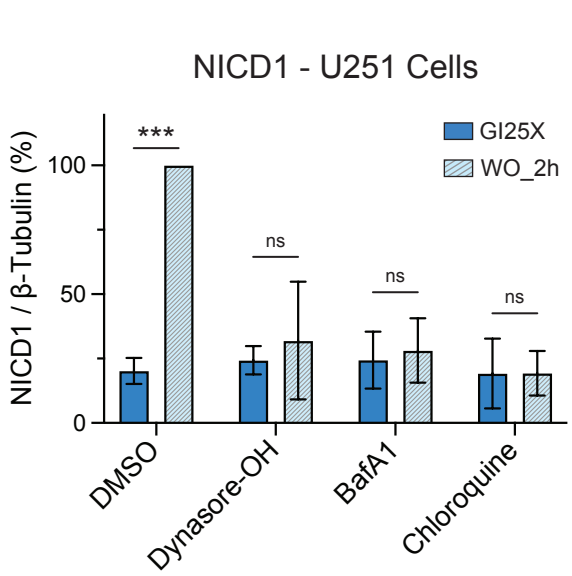

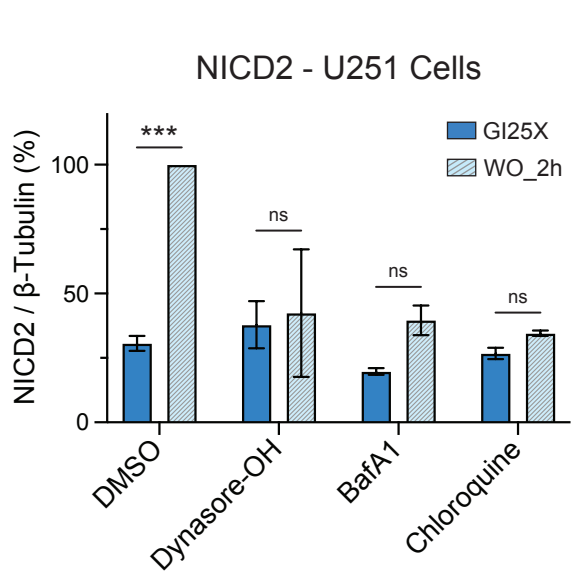

Supplemental Figure 6

A

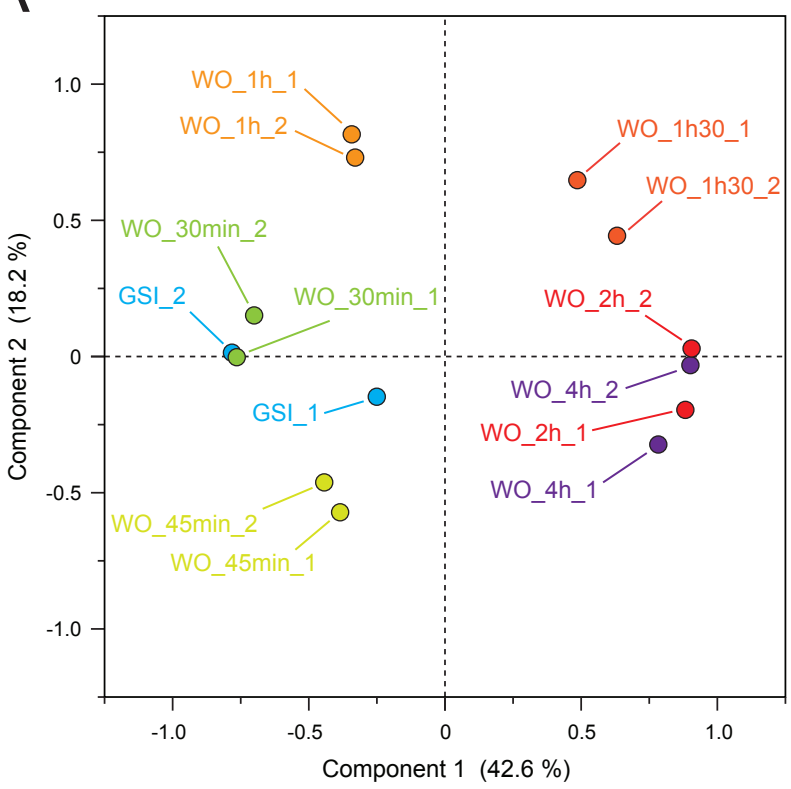

B